

HE 0557–4840 — ULTRA-METAL-POOR AND CARBON-RICH¹

John E. Norris,² N. Christlieb,³ A. J. Korn,⁴ K. Eriksson,⁵ M. S. Bessell,⁶ Timothy C. Beers,⁷ L. Wisotzki,⁸ and D. Reimers⁹

ABSTRACT

We report the discovery and high-resolution, high S/N , spectroscopic analysis of the ultra-metal-poor red giant HE 0557–4840, which is the third most heavy-element deficient star currently known. Its atmospheric parameters are $T_{\text{eff}} = 4900$ K, $\log g = 2.2$, and $[\text{Fe}/\text{H}] = -4.75$. This brings the number of stars with $[\text{Fe}/\text{H}] < -4.0$ to three, and the discovery of HE 0557–4840 suggests that the metallicity distribution function of the Galactic halo does not have a “gap” between $[\text{Fe}/\text{H}] = -4.0$, where several stars are known, and the two most metal-poor stars, at $[\text{Fe}/\text{H}] \sim -5.3$. HE 0557–4840 is carbon rich – $[\text{C}/\text{Fe}] = +1.6$ – a property shared by all three objects with $[\text{Fe}/\text{H}] < -4.0$, suggesting that the well-known increase of carbon relative to iron with decreasing $[\text{Fe}/\text{H}]$ reaches its logical conclusion – ubiquitous carbon richness – at lowest abundance. We also present abundances (nine) and limits (nine) for a further 18 elements. For species having well-measured abundances or strong upper limits, HE 0557–4840 is “normal” in comparison with the bulk of the stellar population at $[\text{Fe}/\text{H}] \sim -4.0$ – with the possible exception of Co. We discuss the implications of these results for chemical enrichment at the earliest times, in the context of single (“mixing and fallback”) and two-component enrichment models. While neither offers a clear solution, the latter appears closer to the mark. Further data are required to determine the oxygen abundance and improve that of Co, and hence more strongly constrain the origin of this object.

Subject headings: Galaxy: formation — Galaxy: halo — stars: abundances — stars: individual HE 0557–4840 — early Universe — nuclear reactions, nucleosynthesis, abundances

Suggested running title: HE 0557–4840 — ULTRA METAL-POOR AND CARBON-RICH

1. INTRODUCTION

The most metal-poor stars, believed to have formed at redshifts > 5 (see e.g. Clarke & Bromm 2003), and representing well-defined points in space and time, hold clues on the conditions at the earliest epochs that are provided by no other astronomical objects. That is to say, the study of their metallicity distribution function (MDF), together with their relative chemical abundance patterns, have the potential to shed light on the nature of the first generation of objects to form in the Universe, and the manner in which the stellar-made elements (those heavier than Li) first formed.

Consider first the MDF. Four decades after the classic analysis of the archtypical metal-poor stars HD 19445 and HD 140283 by Chamberlain & Aller (1951), it could be claimed (e.g. Ryan & Norris 1991) that the MDF for halo material with¹⁰ $[\text{Fe}/\text{H}] > -4.0$ was in reasonable agreement with the predictions of the simple closed box model of Galactic chemical

¹Based on observations collected at ANU’s 2.3m telescope on Siding Spring Mountain, Australia, and European Southern Observatory, Paranal, Chile (proposal 276.D–5041)

²Research School of Astronomy & Astrophysics, The Australian National University, Mount Stromlo Observatory, Cotter Road, Weston, ACT 2611, Australia; jen@mso.anu.edu.au

³Department of Astronomy and Space Physics, Uppsala University, Box 515, SE-75120 Uppsala, Sweden and Hamburger Sternwarte, University of Hamburg, Gojenbergsweg 112, D-21029 Hamburg, Germany; norbert@astro.uu.se

⁴Department of Astronomy and Space Physics, Uppsala University, Box 515, SE-75120 Uppsala, Sweden; akorn@astro.uu.se

⁵Department of Astronomy and Space Physics, Uppsala University, Box 515, SE-75120 Uppsala, Sweden; kjell.eriksson@astro.uu.se

⁶Research School of Astronomy & Astrophysics, The Australian National University, Mount Stromlo Observatory, Cotter Road, Weston, ACT 2611, Australia; bessell@mso.anu.edu.au

⁷Department of Physics and Astronomy, CSCE: Center for the Study of Cosmic Evolution, and JINA: Joint Institute for Nuclear Astrophysics, Michigan State University, E. Lansing, MI 48824; beers@pa.msu.edu

⁸Astrophysical Institute Potsdam, An der Sternwarte 16, D-14482 Potsdam, Germany; lutz@aip.de

⁹Hamburger Sternwarte, University of Hamburg, Gojenbergsweg 112, D-21029 Hamburg, Germany; dreimers@hs.uni-hamburg.de.

¹⁰ $[\text{Fe}/\text{H}] = \log(\text{N}(\text{Fe})/\text{N}(\text{H}))_{\text{Star}} - \log(\text{N}(\text{Fe})/\text{N}(\text{H}))_{\odot}$, $\log \epsilon(\text{Fe}) = \log(\text{N}(\text{Fe})/\text{N}(\text{H}))_{\text{Star}} + 12.00$

enrichment (the Simple Model) of Searle & Sargent (1972) and Hartwick (1976). Following efforts since that time, however, it has become clear that this is not the case below $[\text{Fe}/\text{H}] < -4.0$: while two objects are currently known at $[\text{Fe}/\text{H}] \sim -5.3$ (HE 0107–5840, Christlieb et al. 2002, 2004, and HE 1327–2326, Frebel et al. 2005; Aoki et al. 2006), the MDF presented by Beers et al. (2005) and the Simple Model lead one to expect some 40 such objects below $[\text{Fe}/\text{H}] = -4.0$. Figure 1, which shows the MDF for the unbiased metal-poor objects that have been the subject of high-resolution, high signal-to-noise (S/N) model-atmosphere (one-dimensional (1D), Local Thermodynamic Equilibrium (LTE)) chemical abundance analyses¹¹, demonstrates a second tantalizing fact. In contrast to the expectation of a continuously decreasing MDF, the two objects at $[\text{Fe}/\text{H}] \sim -5.3$ lie some 1.5 dex below the next most metal-poor objects at $[\text{Fe}/\text{H}] = -4.0$. Despite low numbers, this has led some (e.g. Karlsson 2006) to speak of the possibility of a metallicity “gap” at lowest abundance, which could have profound implications for our understanding of the nature of the first generation of objects that chemically enriched the Galaxy, and presumably the Universe.

Consider next the relative abundance characteristics of the two stars with $[\text{Fe}/\text{H}] \sim -5.3$. Their most distinctive features are the enormous overabundances, relative to iron, of carbon ($[\text{C}/\text{Fe}] \sim 4$), nitrogen ($[\text{N}/\text{Fe}] \sim 2\text{--}4$), and oxygen ($[\text{O}/\text{Fe}] \sim 2\text{--}3$) (see also Bessell et al. 2004 and Frebel et al. 2006). This, taken together with the well-established fact that the incidence of carbon richness increases as one proceeds to lower abundance in the range $-4.0 < [\text{Fe}/\text{H}] < -2.0$ (Beers & Christlieb 2005), suggests that the trend of increasing carbon-richness continues to ubiquitous C enhancement at $[\text{Fe}/\text{H}] \sim -5.0$. Figure 1 shows this trend, where the shaded regions represent objects with $[\text{C}/\text{Fe}] > 1.0$. The simplest explanation of this phenomenon is that the earliest objects in the Universe produced large amounts of CNO relative to Fe, far in excess of the ratios produced at later times. Candidate sites include supernovae with “mixing and fallback” (see Iwamoto et al. 2005, and references therein) and rotating massive stars (Fryer et al. 2001; Meynet et al. 2006). Frebel et al. (2007a) argue that relative overabundances of carbon (and/or oxygen) are necessary below $[\text{Fe}/\text{H}] = -4.0$ to provide the cooling of primordial material via C II and O I at the earliest times to form the low mass stars we observe today. We shall return to this point in §6.2.1

¹¹The samples of stars identified for high-resolution analysis originate from high-proper-motion and objective-prism surveys for metal-poor stars; these samples are expected to suffer no metallicity-dependent bias in their selection for $[\text{Fe}/\text{H}] < -2.0$. The low spectral-resolution prism surveys, which supply the vast majority of stars known with $[\text{Fe}/\text{H}] < -3.0$, are unable to detect the presence of the Ca II K line for all but the very coolest stars. As a result, the possibility of introducing bias into the selection function for the lowest metallicity stars is even more remote. When high-resolution spectra are available one is able to guard against contamination by stellar CH and interstellar Ca II lines that might have militated against recognition of the most metal-poor objects in the discovery phase. See Beers & Christlieb (2005).

Two questions then beg to be addressed. First, is the $-5.3 < [\text{Fe}/\text{H}] < -4.0$ “gap” real, and second, what is the incidence of CNO richness below $[\text{Fe}/\text{H}] < -4.0$? Given the rarity of objects below this limit, one might expect definitive answers to be some time in coming. That said, the purpose of the present paper is to begin the task. We present here the discovery and analysis of HE 0557–4840, a third object having $[\text{Fe}/\text{H}] < -4.0$. In §2 we report its discovery, and the high-resolution, high S/N data obtained to address these questions. Our model-atmosphere analysis of this material to produce accurate chemical abundances is then described in §§3–5. Finally, in §6 we discuss the significance of this object. While much future work remains to be done, we find that the existence of HE 0557–4840 with $[\text{Fe}/\text{H}] = -4.75$ weakens the case for the $-5.3 < [\text{Fe}/\text{H}] < -4.0$ “gap” canvassed above. On the other hand, with $[\text{C}/\text{Fe}] = +1.6$ (and $[\text{N}/\text{Fe}] < +1.5$ and $[\text{O}/\text{Fe}] < +3.1$), the data for HE 0557–4840 are consistent with the suggestion that below $[\text{Fe}/\text{H}] < -4.0$ all stars possess strong enhancement of at least some elements of the CNO group. We summarize our results in §7.

2. OBSERVATIONS

2.1. Discovery

HE 0557–4840 was observed in 2005 December during an observing session on candidate metal-poor stars from the Hamburg/ESO objective-prism survey (HES; Wisotzki et al. 2000) with the Australian National University’s 2.3m telescope/Double Beam Spectrograph combination on Siding Spring Mountain. The spectra were observed with resolving power $R \sim 2000$ and cover the wavelength range 3600–5400 Å. Comparison of the spectrum of HE 0557–4840 with “standard” metal-poor stars also observed during the program immediately revealed it as an object of considerable interest. Figure 2 shows the spectra of HE 0557–4840 and of CD–38° 245, the well-known ultra-metal-poor red giant ($[\text{Fe}/\text{H}] = -4.0$; McWilliam et al. 1995, Norris et al. 2001, Cayrel et al. 2004). Comparison of these spectra shows that the two stars have comparable hydrogen line strength, and therefore similar effective temperature, while the Ca II line is weaker in HE 0557–4840, suggestive of a lower abundance of calcium. Perhaps equally interesting is that the G band of CH at 4300 Å is considerably stronger in HE 0557–4840. Given that CH is not detected in CD–38° 245 ($[\text{C}/\text{Fe}] < -0.3$, Cayrel et al. 2004) it was immediately obvious that HE 0557–4840 is carbon rich relative to CD–38° 245.

This object, with $\alpha(2000) = 05 \text{ h } 58 \text{ m } 39.2 \text{ s}$ and $\delta(2000) = -48^\circ 39' 57''$, and $V = 15.45$ and $B - V = 0.71$ (see §2.3), was clearly a target of interest for high resolution follow-up spectroscopy.

2.2. High-resolution Spectroscopy

HE 0557–4840 was then observed in Service Mode at the Very Large Telescope (VLT) Unit Telescope 2 (UT2) with the Ultraviolet-Visual Echelle Spectrograph (UVES) during the nights of 2006 February 5, 25, and 26 and March 19. Seven individual exposures with an integration time of 1 h each were obtained. UVES was used in dichroic mode with the BLUE390 and RED580 settings. The useful wavelength ranges, in the rest frame of HE 0557–4840, are 3300–4520 Å in the blue-arm spectra, and 4820–5750 Å and 5835–6800 Å in the lower- and upper- red-arm spectra, respectively.

A 1'' slit was used in both arms, yielding a nominal resolving power of $R \sim 40,000$. Since read-out noise was not a limitation, 1×1 pixel binning was employed during the observations, even though this results in a significant oversampling due to the scale of 0.215'' per pixel of the blue-arm CCD and 0.155'' per pixel in the red-arm.

The seven pipeline-reduced spectra were co-added in an iterative procedure in which pixels in the individual spectra affected by cosmic ray hits not fully removed during the data reduction, affected by CCD defects, or other artifacts, were identified. These pixels were flagged and ignored in the final iteration of the co-addition.

The co-added blue-arm spectra, rebinned by a factor of 2, have a maximum S/N per pixel of 120 at 4200 Å, decreasing to $S/N \sim 100$ at the red end. At the blue end, this decreases to $S/N = 60$ at 3700 Å, and $S/N = 15$ at 3300 Å. In the rebinned lower red-arm spectra, the S/N increases linearly from 160 per pixel at 4820 Å to 200 at 5750 Å. It is approximately constant at a level of $S/N = 200$ per pixel throughout the wavelength range covered by the upper red-arm spectra.

2.2.1. Line Strength Measurement

Equivalent widths for HE 0557–4840 were measured independently by the first two authors, using techniques described by Norris et al. (2001) and Christlieb et al. (2004), for unblended lines defined in those investigations, together with that of Cayrel et al. (2004). A comparison of the two data sets is presented in Figure 3, where the agreement is quite satisfactory, with an RMS scatter about the line of best fit of 2.5 mÅ. In the absence of an understanding of the origin of the small departure from the one-to-one line evident in the figure, we have chosen to average the data, and present results for 100 lines suitable for abundance analysis in column (5) of Table 1. The atomic data in the table were mostly

taken from the Vienna Atomic Line Database (VALD¹²; Kupka et al. 1999, Kupka et al. 2000), complemented where necessary by values from the three works cited above. For completeness, we identify in Table 8 of Appendix A a further 45 lines that we regarded as unsuitable for abundance analysis.

2.2.2. Radial Velocities

Heliocentric radial velocities for HE 0557–4840 were measured for the seven individual spectra described above by Gaussian fits of six clean and moderately strong absorption lines. The resulting values are presented in Table 2 where columns (1) and (2) contain the Modified Julian Date and heliocentric velocity, respectively. The mean internal standard error of measurement of a single observation is 0.2 kms^{-1} , while the external error is estimated to be 0.7 kms^{-1} (Napiwotzki et al. 2007).

Given that the dispersion of velocities in the table is 0.21 kms^{-1} , we conclude that to within the accuracy of our measurements the velocity of HE 0557–4840 did not vary over the 43 days of the present observations.

It is interesting to note the large radial velocity, 211.8 kms^{-1} , of HE 0557–4840, in comparison with values of 44.1 kms^{-1} for HE 0107–5240 (Christlieb et al. 2004) and 63.8 kms^{-1} for HE 1327–2326 (Aoki et al. 2006). The large spread in these three values establishes that stars with $[\text{Fe}/\text{H}] < -4.0$ have a velocity dispersion commensurate with that of more metal-rich halo material ($[\text{Fe}/\text{H}] > -4.0$).

2.3. Photometry

In Table 3, we present photometry for HE 0557–4840. The values for the BVR photometry were taken from Beers et al. (2007), while the K magnitudes are from Skrutskie et al. (2006). In this table we also list data for HE 0107–5840 ($[\text{Fe}/\text{H}] = -5.3$) from Christlieb et al. (2004), for comparison purposes. For the reddening of HE 0557–4840 we adopt $E(B - V) = 0.04$ following Schlegel et al. (1998), and the differential relationships $E(V - R) = 0.62E(B - V)$ and $E(V - K) = 3.07E(B - V)$ following Bessell et al. (1998). For HE 0107–5240 we use $E(B - V) = 0.013$.

¹²<http://www.astro.uu.se/~vald/>

3. ATMOSPHERIC PARAMETERS

3.1. Effective Temperature

Following Christlieb et al. (2004), we employ the calibrations of Alonso et al. (1999, 2001) and Houdashelt et al. (2000) to determine effective temperatures for both HE 0557–4840 and HE 0107–5240. Our results are presented in Table 4, where the errors correspond to uncertainties of 0.02, 0.02, and 0.06 mag in $(B - V)_0$, $(V - R)_0$, and $(V - K)_0$, respectively, based on the errors in photometry cited by Beers et al. (2007) and Christlieb et al. (2004), and reasonable errors in reddening. Weighting the values from the three colors in the table by the inverse square of their errors, we find photometric temperatures $T_{\text{eff}} = 5090$ K and 5170 K for HE 0557–4840 and HE 0107–5240, respectively. The present results for HE 0107–5240 agree well with those of Christlieb et al. (2004).

We note that the $(B - V)$ and $(V - R)$ colors indicate insignificant effective-temperature differences between HE 0557–4840 and HE 0107–5240, while the two calibrations of $(V - K)$ point towards an effective-temperature difference of around 300 K between the two objects. The source of this difference is not understood. For completeness, we also note that for HE 0557–4840 $T_{\text{eff}}(V - K) - T_{\text{eff}}(B - V, V - R) \sim -150$ K, while for HE 0107–5240 the corresponding quantity is +170 K.

To constrain the effective temperature further, we compare the observed profiles of $\text{H}\alpha$ and $\text{H}\beta$ with synthetic profiles based on the recipes described in Fuhrmann et al. (1993). While this implementation does not take into account the latest advances in the modelling of the self-broadening of Balmer lines (Barklem et al. 2000), the use of that theory would lower the effective temperature by no more than 50 K, as is evident from the analysis of HE 0107–5240 (Christlieb et al. 2004). Even smaller differences are obtained when the effective temperatures are determined relative to the T_{eff} value derived for the solar Balmer lines in a differential analysis. $\text{H}\alpha$ (see Figure 4) and $\text{H}\beta$ unanimously point towards an effective temperature of 4900 ± 100 K, lending support to the photometric calibrations giving a large (~ 300 K) effective-temperature difference between HE 0557–4840 and HE 0107–5240 (see column (6) of Table 4). While the line strength of $\text{H}\alpha$ directly correlates with gravity, the opposite is true for $\text{H}\beta$ and the higher-order Balmer lines. In addition to determining T_{eff} , the combined analysis of $\text{H}\alpha$ and $\text{H}\beta$ allows one to set constraints on $\log g$ as well (see §3.3).

Given this difference in photometric and spectroscopic effective temperatures, in what follows we shall present abundances for HE 0557–4840 determined for both $T_{\text{eff}} = 4900$ K and 5100 K.

3.2. Microturbulence and Iron Abundance

Using 1D model atmospheres described in §4 below and assuming LTE, we determined the microturbulence velocity ξ_{micr} from 60 Fe I lines by requiring that there be no trend of Fe abundance with line strength. All Fe I lines below 3700 Å were ignored, because the S/N drops rapidly towards shorter wavelengths, resulting in a higher uncertainty of the equivalent width measurements and an increased line-to-line scatter of the Fe I abundance of up to 0.8 dex. The average Fe I abundances are $\log \epsilon = 2.77$ dex and 3.02 dex for $T_{\text{eff}} = 4900$ K and 5100 K, respectively¹³. In both cases, $\xi_{\text{micr}} = 1.8 \text{ km s}^{-1}$.

We also detect two very weak lines of Fe II in our red-arm VLT/UVES spectra. The averaged equivalent widths are 4 mÅ for the line at 5018.44 Å and 8 mÅ for the line at 5169.03 Å. For the latter line, however, spectrum synthesis has to be used to derive an abundance, because the line is blended with a weak Fe I line at 5168.90 Å, having excitation potential $\chi = 0.052$ eV and $\log gf = -3.97$ according to VALD. Taking the blend into account and using atomic data from VALD (see Table 1), the abundances inferred from the two Fe II lines are discrepant by ~ 0.3 dex for $T_{\text{eff}} = 4900$ K. This difference can be partly removed by using “astrophysical” $\log gf$ values for the two lines. That is to say, the $\log gf$ values are determined by fitting the solar spectrum, resulting in values of $\log gf = -1.40$ and -1.30 for Fe II 5018.44 and 5169.03, respectively, where following Asplund et al. (2005) we adopt $\log \epsilon(\text{Fe}) = 7.45$. The abundance difference is then reduced to 0.21 dex.

There is also considerable uncertainty in the measurement of the equivalent widths of these lines, because they are weak, and therefore small changes in the continuum placement have a large effect on the measured line strength. Furthermore, usage of different fitting methods (e.g., using a fixed line width when fitting a Gaussian profile to the line as opposed to leaving the line width as a free parameter during the fit) result in measurements deviating significantly from each other. The uncertainty is illustrated by the fact that the measurements of the 5018.44 Å line by A.J.K. (6.6 mÅ) and N.C. (4.4 mÅ) differ by 2.2 mÅ, translating to an abundance difference of $\Delta \log \epsilon = 0.18$ dex.

In summary, the abundance difference of 0.3 dex can be well-explained by the combined uncertainties of the line strength measurements and $\log gf$ values for the two lines.

The iron abundance determined from Fe II lines is less sensitive to changes of T_{eff} than

¹³ We note for completeness that this procedure does not yield abundances completely independent of excitation potential. Inspection of Table 1, for example, reveals that for $T_{\text{eff}} = 4900$ K $d(\log \epsilon/d\chi \sim -0.2 \text{ dex/eV}$. We have encountered this effect in our analyses of other metal-poor giants, and acknowledge it as a shortcoming of the present 1D analysis.

that from Fe I lines, and therefore the former is less affected by possible systematic errors in the adopted T_{eff} scale. Further, Fe II lines are less affected by non-LTE effects than those of Fe I. For these reasons, we adopt the abundance determined from the two Fe II lines as the Fe abundance of HE 0557–4840.

3.3. Surface Gravity

Establishing the ionization equilibrium of an element is a standard spectroscopic method of deriving the stellar surface gravity. To constrain the surface gravity of HE 0557–4840, we perform a non-LTE analysis using the iron model atom and line data calibrated on local halo stars with good HIPPARCOS parallaxes (Korn et al. 2003). With a mean overionization of +0.11 dex in Fe I, the ionization equilibrium is balanced at 4900 K (from $H\alpha$ and $H\beta$) and $\log g = 2.2$. Assuming an effective temperature of 5100 K, the iron ionization equilibrium would require a much higher gravity, of the order of $\log g = 3$. Such a stellar-parameter combination is in conflict with both the gravity derived from an appropriate isochrone – following the procedure of Christlieb et al. (2004) for HE 0107–5240, one obtains $\log g = 2.2$ – and the constraints of Balmer-profile fitting (see Figure 4). As we shall see in §5.3 the Ca I/Ca II ionization equilibrium at $T_{\text{eff}} = 4900$ K is also consistent with $\log g = 2.2$.

For various reasons (use of a slightly different model atmosphere and gf values, different line selection etc.) the LTE ionization equilibrium was established by N.C. at $\log g = 2.4$; that is, at a higher gravity than indicated by the non-LTE analysis, but without any consideration of overionization. The combination of Balmer-profile temperatures and Fe I/Fe II non-LTE surface gravities was recently shown to yield stellar parameters for metal-poor giant stars in excellent agreement with stellar evolution (Korn et al. 2006). Nonetheless, given the uncertainties arising from the unknown absolute temperature scale of metal-poor stars, we have to accept a potential systematic error in absolute $\log g$ values of up to 0.3 dex.

3.4. Summary

Table 5 summarizes our atmospheric parameters for HE 0557–4840, based on spectroscopic and photometric data. While we consider the purely spectroscopic stellar parameters to be more trustworthy, abundance ratios for both solutions are presented for the reader’s convenience in what follows. The iron abundance for HE 0557–4840 is $[\text{Fe}/\text{H}] = -4.75$ or -4.71 , depending on which of the spectroscopic or photometric solutions, respectively, one prefers.

4. MODEL ATMOSPHERES

We have computed 1D model atmospheres tailored for the abundances of HE 0557–4840; i.e., taking into account in particular the over-abundance of C, as determined during a next-to-final iteration of our abundance analysis. An enhancement of the α -elements, including oxygen, of +0.4 dex, was assumed.

The models were computed with the MARCS code, using opacity sampling in about 100,000 wavelength points. Atomic and diatomic molecular opacities were included in addition to the continuous ones in the model atmosphere computations. The models are hydrostatic, spherically symmetric and computed under the assumption of LTE; convective energy transport is included using a Mixing Length Theory formulation. Further details of the model atmospheres can be found in Gustafsson et al. (2007).

5. ABUNDANCE ANALYSIS

5.1. Atomic features

Following Christlieb et al. (2004), we computed LTE abundances for the transitions in Table 1, using the atomic data and equivalent widths (and their limits) presented there, the atmospheric parameters of Table 5, and the code `eqwi`, version 7.04. The results are presented in columns (6) and (7) of Table 1, for $T_{\text{eff}} = 4900$ K and 5100 K, respectively. For a few lines (in particular those for which only an upper line strength limit appears in Table 1) spectrum synthesis was performed with the code `bsyn`, version 7.04. Figure 5 presents an example of spectrum synthesis in the region of the Sr II 4077.71 line, which was used to confirm the upper limit to the strontium abundance derived by the equivalent width analysis. Spectrum synthesis was also used in the analysis of lines of Li I, Ca I, Ca II, and Fe II (see §3.2).

Co I, with numerous weak lines in the range ~ 3400 – 3600 Å (and hence difficult to measure in HE 0557–4840, given the S/N of the spectra), was analysed by using spectrum co-addition for several lines as described by Frebel et al. (2006) in their analysis of OH lines in HE 1300+0157. (In this method several lines are chosen, the wavelength scale is set to zero at line centre for each line, and the spectra co-added to yield a composite spectrum.) Our adopted application of the technique is shown for the co-addition of the strongest two Co I lines in Figure 6, which presents a comparison of observed and synthetic spectra of HE 0557–4840 and CD–38° 245. (For HE 0557–4840 the synthetic spectra pertain to $T_{\text{eff}} = 4900$ K, while for CD–38° 245 we adopt $T_{\text{eff}} = 4900$ K, $\log g = 2.0$ following

Bessell et al. (2004), $\xi_{\text{micr}} = 2.4 \text{ kms}^{-1}$, $\log \epsilon(\text{Fe II}) = 3.39$ from Christlieb et al. (2007), and $\log \epsilon(\text{Co}) = 1.44$, and hence $[\text{Co}/\text{Fe}] = 0.58$ obtained for the two co-added lines (Christlieb, priv. comm.)). For HE 0557–4840 and CD–38° 245 Figure 6 yields $[\text{Co}/\text{Fe}] = 0.04$ and 0.7, respectively, with the latter in good accord with the result of Christlieb et al. cited above.

Our final results for the atomic lines of 18 elements (ten detections, eight upper limits) are presented in Table 6.

5.2. Molecules

Assuming LTE, we have used spectrum synthesis techniques to seek to analyze features of CH, NH, and CN and constrain the abundances of carbon, nitrogen, and oxygen.

5.2.1. Carbon

The C abundance of HE 0557–4840 was determined from weak to moderately strong CH A-X lines in the wavelength region 4252–4256 Å (see Figure 7), the head of the G band at ~ 4310 Å, the feature at ~ 4323 Å (see Figure 8), and weak lines of the B-X system in the region around Ca II K. We used a line list compiled by B. Plez and A. Jorisson (2006, priv. comm.). The $\log gf$ values and line positions were taken from LIFBASE (Luque & Crosley 1999), and the excitation energies from Jørgensen et al. (1996). The abundances all agree to within 0.05 dex with each other, and we adopt the average of the results, which is listed for both combinations of the stellar parameters in Table 6.

5.2.2. Nitrogen

We determined an upper limit for the nitrogen abundance of HE 0557–4840 by analyzing the (0, 0) band head of the B-X system of CN at 3883 Å (see Figure 9). In these calculations we use a line list of B. Plez (2001, priv. comm.). The details of its computation are described in Hill et al. (2002). We adopt a dissociation energy for the CN molecule of $D_0^0 = 7.76 \text{ eV}$, and the C abundance obtained from the CH lines.

Stronger upper limits can be inferred from the absence of the (0, 0) band head of the A-X system of NH at ~ 3360 Å (see Figure 10), yielding $\log \epsilon(\text{N}) < 4.50$ and < 5.00 for $T_{\text{eff}} = 4900 \text{ K}$ and $T_{\text{eff}} = 5100 \text{ K}$, respectively. For our spectrum synthesis calculations we used the line list of Kurucz (2006) with the $\log gf$ values reduced by 0.3, and a dissociation

energy for NH of $D_0^0 = 3.45 \text{ eV}$. For a discussion of the reasons for the correction of the $\log gf$ values and the choice of D_0^0 see Johnson et al. (2007).

5.2.3. Oxygen

In Table 6, we have listed upper limits for the oxygen abundance, derived from the upper limit to the line strength of the O I line at 6300.30 \AA . Due to our VLT/UVES spectrum beginning only at 3300 \AA it was not possible to determine the oxygen abundance from the UV OH A-X lines.

5.3. Calcium in non-LTE

As well as iron, calcium is also observed in two ionization stages. This offers the possibility of checking the spectroscopic stellar-parameter determination, primarily the gravity, independently. As can be seen from the three calcium-line entries of Table 1, the two ionization stages indicate significantly different LTE abundances. For the $T_{\text{eff}} = 4900 \text{ K}$ case, $\log \epsilon (\text{Ca I } 4226) = 1.81$ and $\log \epsilon (\text{Ca II } 3933) = 2.26$. The abundance derived from the subordinate line Ca II 3706 falls in between $-\log \epsilon (\text{Ca II } 3706) = 2.11$ with some added uncertainty arising from blends with CH. The situation is similar for the $T_{\text{eff}} = 5100 \text{ K}$ solution, albeit at higher calcium abundances.

According to computations by Mashonkina et al. (2007), both Ca I 4226 and Ca II 3706 are affected by non-LTE. Such corrections raise the abundances derived from these lines by $\sim +0.30$ and $+0.17 \text{ dex}$, respectively. The non-LTE corrections are similar for both solutions. While this brings the two observed Ca II lines into excellent agreement for the $T_{\text{eff}} = 4900 \text{ K}$ solution, the predicted non-LTE effect for Ca I 4226 is too small to establish the ionization equilibrium (by 0.2 dex). Thus, while the two lines of Ca II can be reconciled at 4900 K , the ionization equilibrium seems to ask for a significantly lower surface gravity than $\log g = 2.2$.

For the $T_{\text{eff}} = 5100 \text{ K}$ solution, the non-LTE abundance of Ca I 4226 is 0.07 dex larger than that derived from Ca II 3706. This indicates that the gravity would have to be raised by about 0.3 dex to establish the ionization equilibrium. At these stellar parameters, Ca II 3933 would yield an abundance 0.18 dex above the other two lines. The corresponding trend in abundance versus excitation energy in Ca II is reminiscent of similar trends seen in Fe I for metal-poor stars including HE 0557–4840 and could indicate deficits in the $T-\tau$ relation of hydrostatic model atmospheres.

Table 7 indicates how the situation would change, for $T_{\text{eff}} = 4900 \text{ K}$, if the analysis were

done differentially with respect to the Sun employing the methodology and gf values favored by Mashonkina et al. (2007). Column (2) presents the non-LTE corrections discussed above, while columns (3) and (4) give the changes due to different gf values, and fitting to the Sun, respectively. (Since both lines of Ca II are very strong and heavily blended in the solar spectrum, no attempt was made to derive astrophysical gf values for them. In these cases, only the corrections given in columns (2) and (3) were employed.) The final calcium abundances are presented in column (5).

As can be seen, the ionization equilibrium of Ca I 4226 and the $\log g$ -sensitive line Ca II 3706 can be established to within 0.03 dex at $T_{\text{eff}} = 4900$ K. The three lines then indicate a calcium abundance $\log \epsilon (\text{Ca}) = 2.22 \pm 0.03$ (1σ). For the $T_{\text{eff}} = 5100$ K solution, the abundance from Ca I 4226 is 0.25 dex larger than that from Ca II 3706. This would require a substantially (~ 1 dex) larger $\log g$ (cf. §3.3). Accordingly, the abundances from the three lines scatter significantly more – $\log \epsilon (\text{Ca}) = 2.39 \pm 0.14$, if $\log g = 2.2$ is assumed.

We conclude that, within the uncertainties of the present analysis, it is possible to establish the Fe I/Fe II and Ca I/Ca II ionization equilibria at $T_{\text{eff}} = 4900$ K and $\log g = 2.2$, while this is not the case for $T_{\text{eff}} = 5100$ K and $\log g = 2.2$. Adding Balmer-profile analyses to the picture, we therefore favour the $T_{\text{eff}} = 4900$ K solution. We note that the chosen stellar-parameter determination thus employs techniques very similar to those used in the analysis of HE 0107–5240 (Christlieb et al. 2004), putting the chemical abundances of both stars on the same abundance scale and making possible a differential analysis.

5.4. Abundance Errors

Abundance errors, within the 1D, LTE formalism adopted here, have been discussed in considerable detail by Christlieb et al. (2004) for HE 0107–5240, to which we refer the reader. Given the similarity of temperatures and gravities of that object and HE 0557–4840, we shall not repeat the discussion here, except to note that random abundance errors introduced by uncertainties of the measurements of equivalent widths in a spectrum of the quality that we use here are typically of the order of 0.1 dex, and those caused by uncertainties of atomic data are typically of the order of 0.10–0.15 dex. Systematic errors of the stellar parameters, most notably T_{eff} , can easily result in systematic difference in the *absolute* abundances of 0.2 dex, while these errors mostly cancel out for abundance *ratios* of atomic species of the same ionization state having similar ionization potentials (e.g., [Ti II/Fe II], or [Ni I/Fe I])

Non-LTE corrections are metallicity dependent and can become quite large in extremely

metal-poor stars (especially giants), in particular for resonance lines of photoionization-dominated minority species. This is, for example, the case for Ca I 4226 for which the non-LTE correction is $\sim +0.5$ dex for HE 1327–2326. Smaller corrections are expected for lines arising from transitions within dominant ionization stages. However, for subordinate lines corrections can reach ~ 0.2 dex (cf. Ca II 3706 as discussed in §5.3).

Finally, in extremely metal-poor giants, the work of Collet et al. (2006) shows that the use of 3D, LTE modeling (as opposed to our 1D, LTE procedure) will lead to significantly lower abundances than reported here. In column (6) of Table 6 we present their results for the corrections $\Delta \log \epsilon(X) = \log \epsilon(X)_{3D} - \log \epsilon(X)_{1D}$ for HE 0107–5240 (which has very similar T_{eff} and $\log g$ to those of HE 0557–4840). Roughly speaking, our abundances derived from diatomic molecules are too high by ~ 1.0 dex, while for atomic species our values are too large by -0.1 to 0.5 , with most values in the range $0.1 - 0.3$. That said, one should note the caveat of Collet et al. (2006) in the context of the iron peak elements: “We caution ... that the neglected non-LTE effects might actually be substantial ...”

6. DISCUSSION

While Table 6 presents abundances for both $T_{\text{eff}} = 4900$ K and $T_{\text{eff}} = 5100$ K, for reasons stated above, our preference is for the former. Accordingly, we shall use results for $T_{\text{eff}} = 4900$ K in what follows.

6.1. The Low-metallicity Tail of the Metallicity Distribution Function

With $[\text{Fe}/\text{H}] = -4.75$, HE 0557–4840 falls midway between the most metal-poor objects at $[\text{Fe}/\text{H}] \sim -5.3$ (HE 0107–5240 and HE 1327–2326), on the one hand, and the several next metal-poor stars at $[\text{Fe}/\text{H}] -4.0$, on the other. *Our first conclusion is that the discovery of HE 0557–4840 weakens the case for a “gap” in the metallicity distribution function (MDF) between $[\text{Fe}/\text{H}] = -4.0$ and -5.3 .*

We also note that although the search for metal-poor stars in the HES is not yet complete, the survey has already increased the total number of known metal-poor stars by more than a factor three with respect to all previous surveys combined for such objects, and all three stars currently known to have $[\text{Fe}/\text{H}] < -4.0$ were discovered in the HES. This suggests that the previously suspected absence of stars at $[\text{Fe}/\text{H}] < -4.0$, as well as the presence of the putative “gap” in the MDF were statistical artifacts caused by too small samples of metal-poor stars. If this explanation is correct, it is expected that the follow-up observa-

tions of the remaining HES metal-poor candidates, and even deeper surveys, such as SEGUE (see e.g. <http://www.sdss.org/segue> and the description in Beers & Christlieb 2005), will further populate the “gap”, as well as the metallicity region below $[\text{Fe}/\text{H}] = -5.0$.

The shape of the low-metallicity tail of the MDF of the Galactic halo contains information on the earliest phases of its chemical enrichment. Prantzos (2003), for example, compares a preliminary MDF derived from the results of spectroscopic follow-up observations of candidate metal-poor stars from the HK survey (see e.g. Beers et al. (2007) for details of the survey) with three different models of galactic chemical evolution. He finds that the low-metallicity tail is reproduced well by a “simple outflow model” with a relaxed Instantaneous Recycling Approximation (IRA) and the assumption of an early phase of infall of primordial gas lasting about 0.2 Gyr. The latter assumption reduces the number of stars at $[\text{Fe}/\text{H}] < -3.0$ relative to “simple outflow” models without early infall and with or without IRA. Such a reduction is adopted to match the observed MDF. The model predicts, however, an MDF increasing continuously from the lowest $[\text{Fe}/\text{H}]$ to the peak of the MDF at around $[\text{Fe}/\text{H}] = -1.6$. From Figure 1 of Prantzos (2003), one sees that the number of stars in the range $-5.0 < [\text{Fe}/\text{H}] < -4.0$ should be about five times as high as the number having $[\text{Fe}/\text{H}] < -5.0$. Since there are now two stars known with $[\text{Fe}/\text{H}] < -5.0$, about ten stars should have been found in the previously suspected “gap” of the MDF – while in reality only one has been identified (HE 0557–4840).

Similar problems arise for the galaxy formation and chemical evolution model of Salvadori et al. (2007). A critical metallicity Z_{cr} for low-mass (i.e., $M < 1 M_{\odot}$) star formation as low as $Z_{\text{cr}} = 10^{-5} Z_{\odot}$ would have to be adopted in order to reproduce the number of stars at $[\text{Fe}/\text{H}] < -5.0$ (i.e., two) correctly, but this would result in a large number of objects in the regime $-5.0 < [\text{Fe}/\text{H}] < -4.0$, in contradiction with the observations.

Karlsson (2006) considered a stochastic chemical enrichment model for the Galactic halo in which negative feedback effects, from the first generation of (massive) stars that formed from primordial gas clouds, resulted in a suppression of all star formation. Later, at redshifts of about $z = 5$, the second generation of stars formed from gas pre-enriched to levels of $[\text{Fe}/\text{H}] < -5.0$ by the previous generation of stars that exploded as Type-II supernovae (SN II). (The resulting mass function had a bias towards high mass (short-lived) stars except where carbon was sufficiently overabundant with respect to iron to allow low mass (long-lived) objects to form.) The MDF resulting from this model has one (or more) “pre-enrichment” peaks in the range $-5.5 < [\text{Fe}/\text{H}] < -5.0$, with the number of stars then first decreasing with increasing $[\text{Fe}/\text{H}]$, until it rises again at $[\text{Fe}/\text{H}] > -4.0$.

The MDF of Karlsson matches the observations reasonably well. In his most favourable case, with suppression of star formation in carbon-deficient gas, some 3–4 objects are pre-

dicted in the range $-5.1 < [\text{Fe}/\text{H}] < -4.2$. The observational constraints on the exact form of the MDF at the lowest metallicities are, however, still weak, since currently only three stars having $[\text{Fe}/\text{H}] < -4.0$ are known. Ongoing and future surveys for metal-poor stars, expected to lead to the identification of significant numbers of new stars at the lowest metallicities as noted above, should clarify the situation.

A particularly interesting and exciting prediction of Karlsson’s model is that there is an additional, smaller peak in the MDF at around $[\text{Fe}/\text{H}] = -7.0$. From his Figure 2, one can estimate that among ten stars at $[\text{Fe}/\text{H}] < -5.0$ there should be one at $[\text{Fe}/\text{H}] \sim -7.0$ ¹⁴

6.2. Relative Abundances

Figure 11 presents $[\text{X}/\text{Fe}]$ as a function of $[\text{Fe}/\text{H}]$ for 12 representative elements (X) in HE 0557–4840 and the other ~ 50 metal-poor stars with $[\text{Fe}/\text{H}] < -3.0$ for which high-resolution, high S/N abundance analyses exist. The comparison data have been taken with first preference from Aoki et al. (2002, 2004, 2006), Bessell et al. (2004), Carretta et al. (2002), Cayrel et al. (2004), Christlieb et al. (2004), Cohen et al. (2004), François et al. (2003), Frebel et al. (2007b), Norris et al. (1997, 2000, 2001, 2002), and Plez & Cohen (2005), supplemented by earlier material from McWilliam et al. (1995) and Ryan et al. (1991, 1996). In the figure, HE 0557–4840 is represented by a filled star, HE 1300+0157 (Frebel et al.) by an open one, results of Cayrel et al. and François et al. by filled circles, and others by open ones.

It is important to note that all of the data in the figure have been determined using 1D model atmospheres and the assumption of LTE. This should be borne in mind when comparison is made with predictions of stellar evolution and galactic chemical enrichment models.

We note in passing that in Figure 11 there are six pairs of related elements – representing the CNO group, the light odd-numbered elements, the α -elements, the Fe-peak below (Cr

¹⁴One should also bear in mind the possible role of accretion onto the most metal-poor stars of more “normal” abundance material from the Galactic ISM over some 13 Gyr, as discussed, for example, by Yoshii (1981) and Iben (1983). The latter predicted that such effects could raise the iron abundance in the outer layers of red giants from zero to $[\text{Fe}/\text{H}] = -5.7$. We refer the reader also to the discussion by Christlieb et al. (2004) who considered possible maximal accretion onto HE 0107–5240, and concluded that “most heavy elements of HE 0107–5240 *might* be accreted from the interstellar medium, although this is most probably not the case for C, N, and Na”. What remains to be addressed is whether minimal accretion conditions existed that would permit one to recognize objects that initially had $[\text{Fe}/\text{H}] = -7.0$.

and Mn) and above (Co and Ni) iron, and the heavy neutron-capture elements.

As has been discussed at some length in a number of the works cited here, and is clear in the figure, the case can be made that for $[\text{Fe}/\text{H}] < -3.0$, and elements with atomic number less than those of the heavy neutron-capture elements, there is a majority fraction that exhibits well-defined trends with small dispersion of $[\text{X}/\text{Fe}]$, together with a minority, C-rich, one that becomes more prominent as one proceeds to lowest abundance and exhibits large enhancements, to varying degrees, of the other lighter elements (N, O, Na, Mg, and Al).

6.2.1. Carbon, Nitrogen, and Oxygen

Inspection of the CNO data for HE 0557–4840 leads to our second important conclusion. *With $[C/\text{Fe}] = +1.65$, $[N/\text{Fe}] < +1.47$, and $[O/\text{Fe}] < +3.09$, HE 0557–4840 belongs to the C-rich group. Currently all objects with $[\text{Fe}/\text{H}] < -4.0$ share this property.*

The question of relative carbon and oxygen overabundance at lowest $[\text{Fe}/\text{H}]$ has been discussed by Frebel et al. (2007a), who address the difficulty of forming low-mass stars, such as HE 0107–5240 and HE 1327–2326, in the early Universe. They argue that cooling by C and O (via fine-structure lines of C II and O I) provides the means of forming objects with $M < 1 M_{\odot}$. They predict that the formation of such low-mass stars will occur due to cooling by C and O if the “transition discriminant” D_{trans} satisfies the condition:

$$D_{\text{trans}} \equiv \log_{10} (10^{[\text{C}/\text{H}]} + 0.3 \times 10^{[\text{O}/\text{H}]}) > -3.5,$$

As may be seen from their Figure 1, both HE 0107–5240 and HE 1327–2326 (with $D_{\text{trans}} \sim -2.7$ to -2.4 , respectively) easily satisfy the condition. For HE 0557–4840 we have a relative overabundance of carbon but only a weak constraint on that of oxygen. If we assume that the latter lies in the range zero to $\log \epsilon_{3\text{D}}(\text{O}) \sim 5.5^{15}$, we obtain $-4.1 < D_{\text{trans}} < -3.5$ for $T_{\text{eff}} = 4900 \text{ K}$. (We adopt $\log \epsilon_{3\text{D}}(\text{C}) - \log \epsilon_{1\text{D}}(\text{C}) = -1.0$, following Collet et al. (2006) for HE 0107–5240.) This range lies close to the limit, but is not inconsistent with the hypothesis of Frebel et al. (2007a). That said, more work is clearly needed to further constrain the abundances of O in HE 0557–4840. A low value for $\log \epsilon(\text{O})$ could marginally challenge their prediction.

¹⁵According to Collet et al. (2006) $\log \epsilon_{3\text{D}}(\text{O}) \sim 5.0$ and 6.0 in HE 0107–5240 and HE 1327–2326, respectively.

6.2.2. The Heavier Elements

Closer inspection of Figure 11 leads to a less exotic, but nevertheless important conclusion. *For all elements other than C, with the possible exception of Co, HE 0557–4840 has $[X/Fe]$ values that differ little from those found in the majority fraction described above.* In this regard HE 0557–4840 is similar to HE 1300+0157 ($[Fe/H] = -3.88$, Frebel et al. 2007b), represented in the figure by the open star. Given the combination of carbon enhancement and low abundances of the heavy neutron-capture elements, it is evident that HE 0557–4840 belongs to the CEMP (Carbon Enhanced Metal Poor)-no group (see Beers & Christlieb 2005), which have carbon enhancement and $[Ba/Fe] < 0.0$ (as does HE 1300+0157).

The Iron Peak

We draw the reader’s attention to the apparently low value of $[Co/Fe]$ for HE 0557–4840 with respect to the bulk of the comparison objects in Figure 11. While one sees, for Cr/Fe and Mn/Fe, that HE 0557–4840 displays the relative underabundances, and for Ni/Fe the solar value, consistent with the trends for extremely metal-poor stars first reported by McWilliam et al. (1995) and Ryan et al. (1996), Co/Fe appears to behave differently¹⁶. That is to say, for HE 0557–4840 one sees $[Co/Fe] = 0.0$, somewhat lower than the value $[Co/Fe] \sim 0.5$ that pertains to the bulk of objects with $[Fe/H] < -3.5$. A word of caution is, however, perhaps in order: inspection of Table 6 shows that for $T_{\text{eff}} = 5100$ K one obtains $[Co/Fe] = 0.3$ for HE 0557–4840. The reader should bear this in mind in the following discussion.

Possible explanations of the relative underabundances of Cr and Mn, the relative overabundance of Co, and the solar behaviour of Ni/Fe for the bulk of extremely metal-poor stars (which demonstrate the need for a possibly wide range of conditions during the explosions of the first stars) include higher than canonical explosion energies (i.e., “hypernovae”, with $> 10^{51}$ ergs) and smaller mass cuts than usually adopted to produce sufficient Fe. A third relevant effect is variation in Y_e , the electron mole number¹⁷. We refer the reader to Umeda & Nomoto (2002, 2005) and Nomoto et al. (2006) for a comprehensive discussion of these points. Suffice it here to say that variation of the explosion energy and of the mass cut

¹⁶We note here for completeness that our spectra, unfortunately, do not encompass the important Zn I lines at 4722.15 and 4810.53 Å, and we are thus unable to seek to determine or set limits on the abundance of this important element.

¹⁷ $Y_e = \sum Z_j X_j / A_j$, where Z_j , X_j , and A_j are the atomic number, mass fraction, and mass number of each species, respectively. Neutron excess is then defined as $\eta = 1 - 2Y_e$

can each act to produce the observed coupled relative underabundance behaviour of [Cr/Fe] and [Mn/Fe], on the one hand, and the relative overabundance one of [Co/Fe], on the other. It is difficult, then, to see how the departure of the [Co/Fe] value in HE 0557–4840 from the general trend might be explained in this manner. In some contrast, varying Y_e on the range 0.4995–0.5005 in an object with $M = 25 M_\odot$, $Z = 10^{-4}$, and $E = 2 \times 10^{52}$ ergs leads to strong decoupling of the nexus between these elements (Umeda & Nomoto 2005, e.g., Figure 4). We shall return to [Co/Fe] (and [Cr/Fe]) in HE 0557–4840 in §6.3.2.

6.3. On the Origin of HE 0557–4840

Given the similarity between the relative abundances of HE 0557–4840 and HE 1300+0157 (their iron abundance difference $\Delta[\text{Fe}/\text{H}] = 0.9$ notwithstanding) we refer the reader to the comprehensive work of Frebel et al. (2007b) who have considered the various possible origins of the latter, and which has great relevance to the present discussion.

6.3.1. The Role of Binarity

The interpretation of the abundance patterns of the most metal-poor stars turns to some extent on their multiplicity. For example, while no significant radial velocity variations have been observed for either of the two most metal-poor stars HE 0107–5240 and HE 1327–2326 ($[\text{Fe}/\text{H}] \sim -5.3$), in the case of the former, Suda et al. (2004) have proposed a Population III, binary model in which HE 0107–5240 is a first generation zero heavy-element object that has experienced binary mass transfer from an asymptotic giant branch (AGB) star, together with accretion from the interstellar medium. A Population II variation on this theme is that HE 0557–4840 could be a second- or later- generation object that has experienced mass transfer from an erstwhile more massive (possibly AGB) companion, leading to enrichment of carbon but not of the heavy neutron-capture elements. See Komiya et al. (2007) for a discussion of this mechanism.

In neither case can such models be excluded as an explanation of HE 0557–4840 by the current level of non-detection of radial velocity variations – as reported in §2.2.2, none has been detected in the present, albeit sparse, data. Future continued radial velocity monitoring is needed to potentially reach a definitive conclusion on its multiplicity.

6.3.2. HE 0557–4840 as a Second or Later Generation Object

The interpretation of HE 0557–4840 with $[\text{Fe}/\text{H}] = -4.8$, and $[\text{C}/\text{Fe}] = +1.6$ as a single, Population II, object requires a scenario in which carbon has been overproduced relative to the heavier elements.

While for HE 0557–4840 one seeks to understand the large C enhancement, our current lack of knowledge concerning the abundances of N and O suggests that one might also consider a more general solution (applicable not only to C but also other light elements) that involves the preferential expulsion, during the explosion of objects with masses greater than $\sim 10 M_{\odot}$, of the outer layers (in which the lighter elements but not the heavier ones have been synthesized), but in which only a small fraction of the inner regions (where the heavier elements have also been produced) is expelled. Some suggestions/models that offer promise in this regard are:

- Rotating, zero-heavy-element ($Z = 0$), very massive ($250\text{--}300 M_{\odot}$) objects (Fryer et al. 2001)
- Failed (low energy), $Z = 0$, supernovae (see e.g. Woosley & Weaver 1995 and Limongi et al. 2003)
- $Z = 0$, $20\text{--}30 M_{\odot}$, “faint” supernovae (explosion energies lower than 10^{51} ergs) with “mixing and fallback” (see Umeda & Nomoto 2003 and Iwamoto et al. 2005)
- Rotating, $Z = 0$, $60 M_{\odot}$ stars (Meynet et al. 2006)

In the context of objects forming from the ejecta of such putative objects, one has also to consider its possible admixture with the existing interstellar medium, which may have already been enriched by the ejecta of less exotic objects, among which one might include non-rotating, energetic core-collapse and pair-instability supernovae in the mass range $10 < M/M_{\odot} < 300$ (see e.g. Woosley & Weaver 1995; Umeda & Nomoto 2002; Heger & Woosley 2002).

Given the approximate nature of the above one dimensional models, it remains to be seen which, if any, of them might be relevant to the enrichment of the material from which HE 0557–4840 and the other C-rich most metal-poor stars formed. That said, the “mixing and fallback” models of Umeda & Nomoto (2003, 2005) reproduce most of the abundance patterns seen in the objects at $[\text{Fe}/\text{H}] \sim -5.3$. The growing number of objects with $[\text{Fe}/\text{H}] < -3.5$ that exhibit relative overabundances of the light elements, together with the diversity of their abundance patterns, are now establishing a challenging framework against which to test and constrain such putative theoretical models.

In the context of HE 0557–4840, stronger limits on oxygen and nitrogen are now required to more rigorously constrain our understanding of its formation and evolution. That said, we noted above that Frebel et al. (2007b) have offered a comprehensive critique of the various models relevant to the manner in which HE 1300+0157 may have formed, which is useful in informing the present discussion of HE 0557–4840. Their basic conclusion was that the CEMP-no abundance pattern of HE 1300+0157 could perhaps result in either of two ways.

Their first scenario envisages enrichment from a single “faint” supernova, with “mixing and fallback” (explosion energies lower than 10^{51} ergs, see e.g. Umeda & Nomoto 2003 and Iwamoto et al. 2005), “with an unusual mass cut allowing for excesses in C and O”. It will be interesting to see whether this versatile type of model can explain the Fe-peak data for HE 0557–4840 in Figure 11. Certainly the mixing and fallback model of Umeda & Nomoto (2003) for the giant HE 0107–5240 (with similar T_{eff} and $\log g$ to those of HE 0557–4840), with $[\text{Co}/\text{Fe}] \sim -1.6$, more than overcomes the problem of low $[\text{Co}/\text{Fe}]$ for HE 0557–4840 discussed in §6.2.2. On the other hand, in that model one finds the prediction of $[\text{Cr}/\text{Fe}] \sim 0.3$, considerably higher than $[\text{Cr}/\text{Fe}]_{3\text{D}} = -1.1$ reported here for HE 0557–4840¹⁸.

Their second suggestion postulates two enrichment sources, with the admixture of ejecta from a massive slowly rotating Population III object ($M > 100 M_{\odot}$, $Z = 0$; see e.g. Heger & Woosley 2002) which produces copious amounts of C and O, but little N and heavier elements before exploding as a pair-instability SN, together with material from a “hypernova” (explosion energy $E \sim 10 \times 10^{51}$ ergs, see e.g. Umeda & Nomoto 2005, and Nomoto et al. 2006) which would contribute heavier elements having atomic number less than 30. There are, however, problems with this model as an explanation of HE 0557–4840. While it is consistent with the observation of $[\text{Co}/\text{Fe}] = 0.76$ in HE 1300+0157, it faces difficulty as an explanation of $[\text{Co}/\text{Fe}] = 0.0$ ($[\text{Co}/\text{Fe}]_{3\text{D}} = -0.3$) in HE 0557–4840, since, as discussed above in §6.2.2, the hypernovae of Umeda & Nomoto (2005) and Nomoto et al. (2006) produce higher Co abundances, for which they report $[\text{Co}/\text{Fe}] \sim 0.4$.

7. Summary

We have reported the discovery and analysis of the ultra metal-poor red giant HE 0557–4840, which has atmospheric parameters $T_{\text{eff}} = 4900$ K, $\log g = 2.2$, and $[\text{Fe}/\text{H}] = -4.75$. This object is also carbon rich, with $[\text{C}/\text{Fe}] = +1.6$, a property shared by the three objects currently known to have iron abundance less than $[\text{Fe}/\text{H}] \sim -4.0$. We have also obtained relative abundances, or abundance limits, for a further 18 elements, and find that,

¹⁸From columns (6) and (8) of Table 6.

with the possible exception of [Co/Fe], HE 0557–4840 has an abundance pattern similar to that of the majority of objects with $[\text{Fe}/\text{H}] \sim -4.0$.

HE 0557–4840 falls in the “gap” between the two most metal-poor stars at $[\text{Fe}/\text{H}] \sim -5.5$ and the next most metal-poor stars at $[\text{Fe}/\text{H}] = -4.0$. Its discovery weakens the case for the existence of such a “gap”. (That said, while the statistics are poor, the number of objects with $-5.0 < [\text{Fe}/\text{H}] < -4.0$ is lower by a factor ~ 3 –4 than predicted at the earliest times by existing models of galactic chemical enrichment.)

The abundance pattern of HE 0557–4840 has been discussed in the context of single and two-component enrichment models. Existing “mixing and fallback” models provide a poor explanation of the observed relative abundances, while a two-component model provides a better, but still inadequate one.

The overabundance of carbon in HE 0557–4840 is (marginally) consistent with the hypothesis of Frebel et al. (2007a) that carbon (and oxygen) richness may be a necessary requirement for formation of low mass stars at the earliest times.

Further data are required to determine the oxygen abundance and improve that of Co, and hence more strongly constrain the origin of HE 0557–4840.

We would like to thank the Director’s Discretionary Time Committee of ESO for allocating time to this project. We express our gratitude to the ESO staff on Paranal and in Garching for carrying out the observations, and reducing the data, respectively. We are grateful to Thomas Szeifert for making it possible for the observations of HE 0107–5240 to be initiated on the night of 5 February, 2006, and to B. Plez and A. Jorissen for providing us with ^{12}CH and ^{13}CH line lists. We also thank Brian Schmidt for beneficial discussion on the kinematics of HE 0557–4840.

J.E.N and M.S.B acknowledge support from the Australian Research Council under grants DP0342613 and DP0663562. N.C. is a Research Fellow of the Royal Swedish Academy of Sciences supported by a grant from the Knut and Alice Wallenberg Foundation. He also acknowledges financial support from Deutsche Forschungsgemeinschaft through grants Ch 214/3 and Re 353/44. A.J.K. and K.E. acknowledge support from Swedish Research Council grants 50349801 and 60307001, respectively. T.C.B. acknowledges partial funding for this work from grants AST 04-06784 and PHY 02-16873: Physics Frontier Center/ Joint Institute for Nuclear Astrophysics (JINA), both awarded by the National Science Foundation.

.

Facilities: ANU:SSO2.3m(DBS); VLT:Kueyen(UVES)

REFERENCES

- Alonso, A., Arribas, S., & Martínez-Roger, C. 1998, *A&AS*, 131, 209
- . 1999, *A&AS*, 140, 261
- Alonso, A., Arribas, S., & Martínez-Roger, C. 2001, *A&A*, 376, 1039
- Aoki, W., Frebel, A., Christlieb, N., Norris, J. E., Beers, T. C., Minezaki, T., Barklem, P. S., Honda, S., Takada-Hidai, M., Asplund, M., Ryan, S. G., Tsangarides, S., Eriksson, K., Steinhauer, A., Deliyannis, C. P., Nomoto, K., Fujimoto, M. Y., Ando, H., Yoshii, Y., & Kajino, T. 2006, *ApJ*, 639, 897
- Aoki, W., Norris, J. E., Ryan, S. G., Beers, T. C., & Ando, H. 2002, *ApJ*, 576, L141
- Aoki, W., Norris, J. E., Ryan, S. G., Beers, T. C., Christlieb, N., Tsangarides, S., & Ando, H. 2004, *ApJ*, 608, 971
- Asplund, M., Grevesse, N., & Sauval, A. J. 2005, in *ASP Conf. Ser.*, Vol. 336, *Cosmic Abundances as Records of Stellar Evolution and Nucleosynthesis in honor of David L. Lambert*, ed. T. G. Barnes & F. N. Bash, San Francisco, 25
- Barklem, P. S., Piskunov, N., & O’Mara, B. J. 2000, *A&A*, 363, 1091
- Beers, T. C. & Christlieb, N. 2005, *ARA&A*, 43, 531
- Beers, T. C., Christlieb, N., Norris, J. E., Bessell, M. S., Wilhelm, R., Allende Prieto, C., Yanny, B., Rockosi, C., Newberg, H. J., Rossi, S., & Lee, Y. S. 2005, in *IAU Symposium*, Vol. 228, *From Lithium to Uranium: Elemental Tracers of Early Cosmic Evolution*, ed. V. Hill, P. François, & F. Primas, 175
- Beers, T. C., Flynn, C., Rossi, S., Sommer-Larsen, J., Wilhelm, R., Marsteller, B., Lee, Y. S., De Lee, N., Krugler, J., Deliyannis, C. P., Simmons, A. T., Mills, E., Zickgraf, F.-J., Holmberg, J., Önehag, A., Eriksson, A., Terndrup, D. M., Salim, S., Andersen, J., Nordström, B., Christlieb, N., Frebel, A., & Rhee, J. 2007, *ApJ Suppl.*, 168, 128
- Bessell, M. S., Castelli, F., & Plez, B. 1998, *A&*, 333, 231
- Bessell, M. S., Christlieb, N., & Gustafsson, B. 2004, *ApJ*, 612, L61
- Carpenter, J. M. 2001, *AJ*, 121, 2851
- Carretta, E., Gratton, R., Cohen, J. G., Beers, T. C., & Christlieb, N. 2002, *AJ*, 124, 481

- Cayrel, R., Depagne, E., Spite, M., Hill, V., Spite, F., François, P., Beers, T. C., Primas, F., Andersen, J., Barbuy, B., Bonifacio, P., Molaro, P., & Nordström, B. 2004, *A&A*, 416, 1117
- Chamberlain, J. W. & Aller, L. H. 1951, *ApJ*, 114, 52
- Christlieb, N., Bessell, M. S., Beers, T. C., Gustafsson, B., Korn, A., Barklem, P. S., Karlsson, T., Mizuno-Wiedner, M., & Rossi, S. 2002, *Nature*, 419, 904
- Christlieb, N., Gustafsson, B., Korn, A. J., Barklem, P. S., Beers, T. C., Bessell, M. S., Karlsson, T., & Mizuno-Wiedner, M. 2004, *ApJ*, 603, 708
- Christlieb, N. et al. 2007, in preparation
- Clarke, C. J. & Bromm, V. 2003, *MNRAS*, 343, 1224
- Cohen, J. G., Christlieb, N., McWilliam, A., Shectman, S., Thompson, I., Wasserburg, G. J., Ivans, I. I., Dehn, M., Karlsson, T., & Meléndez, J. 2004, *ApJ*, 612, 1107
- Collet, R., Asplund, M., & Trampedach, R. 2006, *ApJ*, 644, L121
- François, P., Depagne, E., Hill, V., Spite, M., Spite, F., Plez, B., Beers, T. C., Barbuy, B., Cayrel, R., Andersen, J., Bonifacio, P., Molaro, P., Nordström, B., & Primas, F. 2003, *A&A*, 403, 1105
- Frebel, A., Aoki, W., Christlieb, N., Ando, H., Asplund, M., Barklem, P. S., Beers, T. C., Eriksson, K., Fechner, C., Fujimoto, M. Y., Honda, S., Kajino, T., Minezaki, T., Nomoto, K., Norris, J. E., Ryan, S. G., Takada-Hidai, M., Tsangarides, S., & Yoshii, Y. 2005, *Nature*, 434, 871
- Frebel, A., Christlieb, N., Norris, J. E., Aoki, W., & Asplund, M. 2006, *ApJL*, 638, L17
- Frebel, A., Johnson, J. L., & Bromm, V. 2007a, *ApJ*, submitted, astro-ph/0701139
- Frebel, A., Norris, J. E., Aoki, W., Honda, S., Bessell, M. S., Takada-Hidai, M., Beers, T. C., & Christlieb, N. 2007b, *ApJ*, in press, astro-ph/0612160
- Fryer, C. L., Woosley, S. E., & Heger, A. 2001, *ApJ*, 550, 372
- Fuhrmann, K., Axer, M., & Gehren, T. 1993, *A&A*, 271, 451
- Gustafsson, B., Edvardsson, B., Eriksson, K., Jørgensen, U. G., Nordlund, Å., & Plez, B. 2007, in preparation

- Hartwick, F. D. A. 1976, *ApJ*, 209, 418
- Heger, A. & Woosley, S. E. 2002, *ApJ*, 567, 532
- Hill, V., Plez, B., Cayrel, R., Beers, T. C., Nordström, B., Andersen, J., Spite, M., Spite, F., Barbuy, B., Bonifacio, P., Depagne, E., François, P., & Primas, F. 2002, *A&A*, 387, 560
- Houdashelt, M. L., Bell, R. A., & Sweigart, A. V. 2000, *AJ*, 119, 1448
- Iben, I. Jr. 1983, *Memorie della Societa Astronomica Italiana*, 54, 321
- Iwamoto, N., Umeda, H., Tominaga, N., Nomoto, K., & Maeda, K. 2005, *Science*, 309, 451
- Johnson, J. J., Herwig, F., Beers, T. C., & Christlieb, N. 2007, *ApJ*, in press, astro-ph/0608666
- Jørgensen, U. G., Larsson, M., Iwamae, A., & Yu, B. 1996, *A&A*, 315, 204
- Karlsson, T. 2006, *ApJ*, 641, L41
- Komiya, Y., Suda, T., Minaguchi, H., Shigeyama, T., Aoki, W., & Fujimoto, M. 2007, *ApJ*, in press, astro-ph/0610670
- Korn, A. J., Grundahl, F., Richard, O., Barklem, P. S., Mashonkina, L., Collet, R., Piskunov, N., & Gustafsson, B. 2006, *Nature*, 442, 657
- Korn, A. J., Shi, J., & Gehren, T. 2003, *A&A*, 407, 691
- Kupka, F. G., Piskunov, N., Ryabchikova, T. A., Stempels, H. C., & Weiss, W. W. 1999, *A&AS*, 138, 119
- Kupka, F. G., Ryabchikova, T. A., Piskunov, N., Stempels, H. C., & Weiss, W. W. 2000, *Baltic Astronomy*, 9, 590
- Kurucz, R. 2006, <http://kurucz.harvard.edu/LINELISTS/LINESMOL>
- Limongi, M., Chieffi, A., & Bonifacio, P. 2003, *ApJ*, 594, L123
- Luque, J. & Crosley, D. R. 1999, LIFBASE version 1.5, Sri international report mp 99-009, SRI International, <http://www.sri.com/cem/lifbase/Lifbase.PDF>
- Mashonkina, L., Korn, A. J., & Przybilla, N. 2007, *A&A*, 461, 261
- McWilliam, A., Preston, G. W., Sneden, C., & Searle, L. 1995, *AJ*, 109, 2757

- Meynet, G., Ekström, S., & Maeder, A. 2006, *A&A*, 447, 623
- Napiwotzki, R. et al. 2007, in preparation
- Nomoto, K., Tominaga, N., Umeda, H., Kobayashi, C., & Maeda, K. 2006, *Nuc.Phys.A*, 777, 424, astro-ph/0605725
- Norris, J. E., Beers, T. C., & Ryan, S. G. 2000, *ApJ*, 540, 456
- Norris, J. E., Ryan, S. G., & Beers, T. C. 1997, *ApJ*, 489, L169
- . 2001, *ApJ*, 561, 1034
- Norris, J. E., Ryan, S. G., Beers, T. C., Aoki, W., & Ando, H. 2002, *ApJ*, 569, L107
- Plez, B. & Cohen, J. G. 2005, *A&A*, 434, 1117
- Prantzos, N. 2003, *A&A*, 404, 211
- Ryan, S. G. & Norris, J. E. 1991, *AJ*, 101, 1865
- Ryan, S. G., Norris, J. E., & Beers, T. C. 1996, *ApJ*, 471, 254
- Ryan, S. G., Norris, J. E., & Bessell, M. S. 1991, *AJ*, 102, 303
- Salvadori, S., Schneider, R., & Ferrara, A. 2007, *MNRAS*, submitted, astro-ph/0611130
- Schlegel, D. J., Finkbeiner, D. P., & Davis, M. 1998, *ApJ*, 500, 525
- Searle, L. & Sargent, W. L. W. 1972, *ApJ*, 173, 25
- Seaton, M. J., Yan, Y., Mihalas, D., & Pradhan, A. K. 1994, *MNRAS*, 266, 805
- Skrutskie, M. F., Cutri, R. M., Stiening, R., Weinberg, M. D., Schneider, S., Carpenter, J. M., Beichman, C., Capps, R., Chester, T., Elias, J., Huchra, J., Liebert, J., Lonsdale, C., Monet, D. G., Price, S., Seitzer, P., Jarrett, T., Kirkpatrick, J. D., Gizis, J. E., Howard, E., Evans, T., Fowler, J., Fullmer, L., Hurt, R., Light, R., Kopan, E. L., Marsh, K. A., McCallon, H. L., Tam, R., Van Dyk, S., & Wheelock, S. 2006, *AJ*, 131, 1163
- Smith, W. W. & Gallagher, A. 1966, *Phys. Rev.*, 145, 26
- Suda, T., Aikawa, M., Machida, M. N., Fujimoto, M. Y., & Iben, I. Jr. 2004, *ApJ*, 611, 476
- Umeda, H. & Nomoto, K. 2002, *ApJ*, 565, 385

—. 2003, *Nature*, 422, 871

—. 2005, *ApJ*, 619, 427

Wisotzki, L., Christlieb, N., Bade, N., Beckmann, V., Köhler, T., Vanelle, C., & Reimers, D. 2000, *A&A*, 358, 77

Woosley, S. E. & Weaver, T. A. 1995, *ApJS*, 101, 181

Yoshii, Y. 1981, *A&A*, 97, 280

Table 1. AVERAGED EQUIVALENT WIDTHS, UPPER LIMITS, AND LINE-BY-LINE ABUNDANCES OF HE 0557–4840.

Species (1)	λ (Å) (2)	χ (eV) (3)	$\log gf$ (dex) (4)	W_λ (mÅ) (5)	$\log \epsilon_{4900\text{ K}}$ (dex) (6)	$\log \epsilon_{5100\text{ K}}$ (dex) (7)
Li I	6707.761	0.00	−0.009	synth	< 0.70	< 0.90
O I	6300.304	0.00	−9.717	< 5	< 7.00	< 7.13
Na I	5889.951	0.00	0.117	15	1.26	1.44
Mg I	3829.355	2.71	−0.231	49	3.03	3.19
Mg I	3832.304	2.71	0.121	68	3.00	3.16
Mg I	3838.292	2.72	0.392	79	2.95	3.11
Mg I	5172.684	2.71	−0.399	53	3.12	3.30
Mg I	5183.604	2.72	−0.177	64	3.06	3.24
Al I	3961.520	0.01	−0.323	19	1.01	1.22
Ca I	4226.728	0.00	0.265	synth	1.81	2.03
Ca II	3706.024	3.12	−0.480	synth	2.11	2.12
Ca II	3933.663	0.00	0.105	synth	2.26	2.51
Sc II	3572.526	0.02	0.267	25	−1.54	−1.37
Sc II	3576.340	0.01	0.007	21	−1.38	−1.21
Sc II	3580.925	0.00	−0.149	20	−1.26	−1.09
Sc II	3642.784	0.00	0.133	26	−1.39	−1.21
Ti II	3759.296	0.61	0.270	68	0.38	0.51
Ti II	3761.323	0.57	0.170	65	0.37	0.50
Ti II	3900.551	1.13	−0.280	21	0.53	0.64
Ti II	3913.468	1.12	−0.410	20	0.63	0.74
Ti II	4395.033	1.08	−0.510	17	0.55	0.66
Ti II	4443.794	1.08	−0.700	12	0.55	0.66
Cr I	3578.684	0.00	0.409	16	0.19	0.46
Cr I	4254.332	0.00	−0.114	7	0.18	0.43
Mn I	4030.753	0.00	−0.470	< 10	< 0.01	< 0.29
Fe I	3727.619	0.96	−0.631	56	2.69	2.94
Fe I	3743.362	0.99	−0.785	49	2.71	2.96
Fe I	3745.561	0.09	−0.771	97	2.91	3.21

Table 1—Continued

Species (1)	λ (Å) (2)	χ (eV) (3)	$\log gf$ (dex) (4)	W_λ (mÅ) (5)	$\log \epsilon_{4900\text{ K}}$ (dex) (6)	$\log \epsilon_{5100\text{ K}}$ (dex) (7)
Fe I	3745.900	0.12	−1.335	81	3.04	3.32
Fe I	3758.233	0.96	−0.027	74	2.48	2.73
Fe I	3763.789	0.99	−0.238	67	2.55	2.80
Fe I	3767.192	1.01	−0.389	60	2.56	2.81
Fe I	3787.880	1.01	−0.859	44	2.70	2.95
Fe I	3790.093	0.99	−1.761	11	2.75	3.01
Fe I	3812.964	0.96	−1.047	39	2.72	2.97
Fe I	3815.840	1.49	0.237	61	2.50	2.73
Fe I	3820.425	0.86	0.119	88	2.57	2.83
Fe I	3824.444	0.00	−1.362	85	2.98	3.27
Fe I	3825.881	0.92	−0.037	76	2.45	2.70
Fe I	3827.823	1.56	0.062	53	2.59	2.81
Fe I	3841.048	1.61	−0.045	42	2.52	2.74
Fe I	3849.967	1.01	−0.871	44	2.69	2.93
Fe I	3850.818	0.99	−1.734	12	2.76	3.02
Fe I	3856.372	0.05	−1.286	86	2.98	3.27
Fe I	3859.911	0.00	−0.710	104	2.88	3.19
Fe I	3865.523	1.01	−0.982	39	2.71	2.96
Fe I	3878.018	0.96	−0.914	45	2.69	2.94
Fe I	3878.573	0.09	−1.379	80	2.93	3.22
Fe I	3895.656	0.11	−1.670	69	2.96	3.24
Fe I	3899.707	0.09	−1.531	76	2.96	3.24
Fe I	3902.946	1.56	−0.446	31	2.63	2.86
Fe I	3906.480	0.11	−2.243	43	2.99	3.27
Fe I	3920.258	0.12	−1.746	64	2.93	3.21
Fe I	3922.912	0.05	−1.651	76	3.03	3.31
Fe I	3927.920	0.11	−1.522	78	3.02	3.31
Fe I	3930.297	0.09	−1.491	86	3.17	3.46

Table 1—Continued

Species (1)	λ (Å) (2)	χ (eV) (3)	$\log gf$ (dex) (4)	W_λ (mÅ) (5)	$\log \epsilon_{4900\text{ K}}$ (dex) (6)	$\log \epsilon_{5100\text{ K}}$ (dex) (7)
Fe I	4005.242	1.56	−0.610	26	2.69	2.91
Fe I	4045.812	1.49	0.280	69	2.56	2.79
Fe I	4063.594	1.56	0.062	56	2.60	2.83
Fe I	4071.738	1.61	−0.022	50	2.61	2.84
Fe I	4132.058	1.61	−0.675	20	2.63	2.86
Fe I	4143.868	1.56	−0.511	32	2.68	2.91
Fe I	4202.029	1.49	−0.708	28	2.71	2.94
Fe I	4216.184	0.00	−3.356	9	3.03	3.32
Fe I	4250.787	1.56	−0.714	24	2.70	2.93
Fe I	4260.474	2.40	0.109	16	2.63	2.82
Fe I	4271.761	1.49	−0.164	53	2.64	2.87
Fe I	4294.125	1.49	−1.110	20	2.91	3.14
Fe I	4325.762	1.61	0.006	51	2.58	2.81
Fe I	4375.930	0.00	−3.031	17	3.01	3.30
Fe I	4383.545	1.49	0.200	67	2.55	2.78
Fe I	4404.750	1.56	−0.142	46	2.57	2.80
Fe I	4415.122	1.61	−0.615	27	2.72	2.95
Fe I	4427.310	0.05	−2.924	13	2.80	3.10
Fe I	4920.503	2.83	0.068	6	2.67	2.85
Fe I	5232.940	2.94	−0.058	5	2.77	2.95
Fe I	5269.537	0.86	−1.321	49	2.89	3.15
Fe I	5328.039	0.92	−1.466	35	2.84	3.10
Fe I	5371.490	0.96	−1.645	25	2.87	3.13
Fe I	5397.128	0.92	−1.993	14	2.87	3.13
Fe I	5405.775	0.99	−1.844	19	2.95	3.20
Fe I	5429.697	0.96	−1.879	17	2.88	3.14
Fe I	5434.524	1.01	−2.122	8	2.79	3.05
Fe I	5446.917	0.99	−1.914	14	2.85	3.10

Table 1—Continued

Species (1)	λ (Å) (2)	χ (eV) (3)	$\log gf$ (dex) (4)	W_λ (mÅ) (5)	$\log \epsilon_{4900\text{ K}}$ (dex) (6)	$\log \epsilon_{5100\text{ K}}$ (dex) (7)
Fe I	5455.610	1.01	−2.091	11	2.94	3.20
Fe II	5018.440	2.89	−1.220	4	2.53	2.57
Fe II	5169.033	2.89	−1.303	synth	2.86	2.90
Ni I	3414.760	0.03	−0.014	66	1.05	1.35
Ni I	3423.704	0.21	−0.760	30	1.16	1.45
Ni I	3433.554	0.03	−0.668	47	1.22	1.52
Ni I	3452.885	0.11	−0.910	35	1.32	1.61
Ni I	3610.461	0.11	−1.149	28	1.38	1.67
Ni I	3783.524	0.42	−1.310	10	1.32	1.59
Ni I	3807.138	0.42	−1.205	12	1.28	1.55
Ni I	3858.292	0.42	−0.936	21	1.30	1.56
Sr II	4077.709	0.00	0.167	< 10	< −2.90	< −2.75
Y II	3788.700	0.10	−0.070	< 10	< −1.80	< −1.64
Zr II	4211.907	0.53	−1.083	< 10	< 0.11	< 0.25
Ba II	4934.076	0.00	−0.150	< 10	< −2.55	< −2.37
Eu II	4129.725	0.00	0.173	< 10	< −2.19	< −2.03

Table 2. RADIAL VELOCITIES OF HE 0557–4840.

MJD	V_r
	kms^{-1}
(1)	(2)
53771.029	211.44
53771.072	211.67
53771.159	211.61
53791.025	211.98
53792.035	211.90
53792.078	212.02
53813.999	211.84

Table 3. BROAD-BAND PHOTOMETRY OF HE 0107–5240 AND HE 0557–4840.

Object	V	$B - V$	$V - R$	K	$V - K$
(1)	(2)	(3)	(4)	(5)	(6)
HE 0107–5240	15.17 ^a	0.69 ^a	0.44 ^a	13.24 ^a	1.93 ^a
HE 0557–4840	15.454 ^b	0.712 ^b	0.463 ^b	13.194 ^c	2.254 ^d

^aFrom Christlieb et al. (2004, Table 2, “adopted” values)

^bFrom Beers et al. (2007); errors in V , $B - V$ and $V - R$ are 0.004, 0.008, and 0.006, respectively

^cFrom 2MASS (Skrutskie et al. 2006); error is 0.037

^dOn the Johnson-Glass system; error is 0.037

Table 4. DERIVATION OF T_{eff} FOR HE 0557–4840 AND HE 0107–5240.

Measured ^a quantity (1)	HE 0557–4840		HE 0107–5240		ΔT_{eff} (K) (6)	References ^b (7)
	Value (2)	Derived T_{eff} (K) (3)	Value (4)	Derived T_{eff} (K) (5)		
$H\alpha$...	4900 ± 100	...	5180 ± 70	–280	1
$(B - V)_0/\text{J}$	0.672	5170 ± 50	0.680	5150 ± 50	20	2
$(V - R)_0/\text{C}$	0.438	5140 ± 100	0.434	5170 ± 100	–30	2
$(V - K)_0/\text{JG}$	2.125	5060 ± 70	1.884	5340 ± 80	–280	2
$(B - V)_0/\text{J}$	0.672	5110 ± 60	0.680	5080 ± 60	30	3
$(V - K)_0/\text{JTCS}$	2.179	4920 ± 70	1.935	5230 ± 80	–310	3

^aColors with qualifiers J, C, and JG refer to the Johnson, Cousins, and Johnson-Glass systems, respectively. JTCS refers to $V - K$ colors, where transformation from 2MASS to Johnson-Glass was effected by using the transformations of Carpenter (2001) and thence to the TCS system following Alonso et al. (1998)

^bReferences – (1) Fuhrmann et al. (1993); (2) Houdashelt et al. (2000); (3) Alonso et al. (1999, 2001)

Table 5. STELLAR PARAMETERS FOR HE 0557–4840.

Parameter (1)	Spectroscopy		Photometry	
	Value (2)	σ^a (3)	Value (4)	σ^a (5)
T_{eff} (K)	4900	100	5100	50
$\log g$ (cgs)	2.2	0.3	2.2	0.3
[Fe/H]	−4.8	0.2	−4.7	0.2
ξ_{micr} (km s ^{−1})	1.8	0.2	1.8	0.2

^aInternal error estimate

Table 6. 1D LTE ABUNDANCES OF HE 0557–4840.

Spec- ies (1)	N_{lines} (2)	$\log \epsilon(\text{X})$ (4900 K) (3)	$\log \epsilon(\text{X})$ (5100 K) (4)	$\sigma_{\log \epsilon}$ ^a (5)	3D ^b Corr. (6)	$\log \epsilon(\text{X})_{\odot}$ ^c (7)	$[\text{X}/\text{Fe}]^{\text{d}}$ (4900 K) (8)	$[\text{X}/\text{Fe}]^{\text{e}}$ (5100 K) (9)	Notes (10)
Li I	1	< 0.70	< 0.90	...	−0.2	synthesis
C(CH)	...	5.29	5.76	0.10	~ −1.0	8.39	+1.65	+2.08	A-X & B-X
N(CN)	...	< 5.40	< 5.60	0.10	~ −2.2	7.78	< +2.37	< +2.53	B-X
N(NH)	...	< 4.50	< 5.00	0.20	~ −1.0	7.78	< +1.47	< +1.93	A-X
O I	1	< 7.00	< 7.13	8.66	< +3.09	< +3.18	
Na I	1	1.26	1.44	...	−0.1	6.17	−0.16	−0.02	
Mg I	5	3.03	3.20	0.07	−0.1	7.53	+0.25	+0.38	
Al I	1	1.01	1.22	...	−0.1	6.37	−0.61	−0.44	
Ca I	1	1.81	2.03	...	−0.2	6.31	+0.25	+0.43	
Ca II	2	2.18	2.32	...	−0.2	6.31	+0.62	+0.72	
Sc II	4	−1.39	−1.22	0.11	−0.1	3.05	+0.31	+0.44	
Ti II	5	0.50	0.62	0.10	0.0	4.90	+0.35	+0.43	
Cr I	2	0.19	0.44	...	−0.3	5.64	−0.70	−0.49	
Mn I	1	< 0.01	< 0.29	...	−0.4	5.39	< −0.63	< −0.39	
Fe I	60	2.77	3.02	0.17	−0.2	7.45	+0.07	+0.28	
Fe II	2	2.70	2.74	...	+0.1	7.45	
Co I	2	0.20	0.50	...	−0.3	4.92	+0.04	+0.30	co-addition
Ni I	8	1.26	1.54	0.10	−0.3	6.23	−0.22	+0.02	
Sr II	1	< −2.90	< −2.75	...	−0.2	2.92	< −1.07	< −0.98	
Y II	1	< −1.80	< −1.64	2.21	< +0.74	< +0.86	
Zr II	1	< 0.11	< 0.25	2.59	< +2.27	< +2.37	
Ba II	1	< −2.55	< −2.37	...	−0.3	2.17	< +0.03	< +0.17	
Eu II	1	< −2.19	< −2.03	...	−0.5	0.52	< +2.04	< +2.16	

^aUncertainty of the fit in the case of spectrum synthesis; standard deviation of the mean for abundances determined from equivalent width measurements of $N > 2$ lines

^b3D Corr. = $\log \epsilon(\text{X})_{\text{3D}} - \log \epsilon(\text{X})_{\text{1D}}$, following Collet et al. (2006) for HE 0107–5240

^cFrom Asplund et al. (2005)

^dAdopting an Fe abundance of $[\text{Fe}/\text{H}] = -4.75$, as derived from Fe II

^eAdopting an Fe abundance of $[\text{Fe}/\text{H}] = -4.71$, as derived from Fe II

Table 7. ABUNDANCE CHANGES AND $\log \epsilon$ (Ca) FOR $T_{\text{eff}} = 4900$ K, FOLLOWING MASHONKINA ET AL. (2007).

Line	$\log \epsilon$ (non-LTE) – $\log \epsilon$ (LTE)	$\log \epsilon$ ($\log gf$) – $\log \epsilon$ (LTE)	$\log \epsilon$ (solar fit) – $\log \epsilon$ (LTE)	$\log \epsilon$ (Ca) _{Diff} ^{non-LTE} (4900 K)
(1)	(2)	(3)	(4)	(5)
Ca I 4226	+0.26	+0.02 ^a	+0.10	2.19
Ca II 3706	+0.17	–0.06 ^b	... ^c	2.22
Ca II 3933	0.00	–0.02 ^b	... ^c	2.24

^aFrom Smith & Gallagher (1966)

^bFrom the Opacity Project (Seaton et al. 1994)

^cNo solar fitting attempted due to strong blending

A. Rejected lines

In Table 8 we list absorption lines that were excluded from the abundance analysis for various reasons. In the case of rejections based on visual inspection of a line in the VLT/UVES spectrum, it was rejected when either N.C. or J.E.N. (or both) suspected it to be blended.

Table 8. REJECTED ABSORPTION LINES.

Species (1)	λ (\AA) (2)	χ (eV) (3)	$\log gf$ (dex) (4)	Reason for rejection (5)
Na I	5895.924	0.000	−0.184	Blended ^a
Si I	3905.523	1.909	−1.090	Blended ^a
Sc II	3613.829	0.022	0.416	Blended ^a
Sc II	3630.742	0.008	0.220	Blended ^a
Ti II	3444.314	0.151	−0.810	Blended ^a
Ti II	3477.187	0.122	−0.967	Blended ^a
Ti II	3491.066	0.113	−1.060	Blended ^a
Ti II	3641.331	1.237	−0.710	Blended ^a
Ti II	3685.19	0.574	−0.040	Affected by Balmer line
Ti II	3814.584	0.574	−1.700	Blended ^a
Fe I	3440.606	0.000	−0.673	low S/N
Fe I	3440.989	0.052	−0.958	low S/N
Fe I	3443.877	0.087	−1.374	low S/N
Fe I	3475.450	0.087	−1.054	low S/N
Fe I	3476.702	0.121	−1.507	low S/N
Fe I	3490.574	0.052	−1.105	low S/N
Fe I	3497.841	0.110	−1.549	low S/N
Fe I	3521.261	0.915	−0.988	low S/N
Fe I	3558.515	0.990	−0.629	low S/N
Fe I	3565.379	0.958	−0.133	low S/N
Fe I	3581.193	0.859	0.406	low S/N
Fe I	3585.705	0.915	−1.187	low S/N
Fe I	3586.985	0.990	−0.796	low S/N
Fe I	3608.859	1.011	−0.100	low S/N
Fe I	3618.768	0.990	−0.003	low S/N
Fe I	3631.463	0.958	−0.036	low S/N
Fe I	3647.843	0.915	−0.194	low S/N
Fe I	3705.57	0.052	−1.334	Affected by Balmer line
Fe I	3709.25	0.915	−0.646	Affected by Balmer line

Table 8—Continued

Species (1)	λ (Å) (2)	χ (eV) (3)	$\log gf$ (dex) (4)	Reason for rejection (5)
Fe I	3795.002	0.990	−0.761	Blended ^a
Fe I	3840.44	0.990	−0.506	Affected by Balmer line
Fe I	3872.50	0.991	−0.910	Blended ^a
Fe I	4238.02	3.417	−1.286	Blended with a CH line
Co I	3873.114	0.432	−0.660	Blended with a CH line
Ni I	3413.472	0.165	−1.480	Blended ^a
Ni I	3437.275	0.000	−1.192	Blended ^a
Ni I	3472.542	0.109	−0.810	Blended ^a
Ni I	3483.770	0.275	−1.110	Blended ^a
Ni I	3492.954	0.109	−0.250	Blended ^a
Ni I	3500.846	0.165	−1.279	Blended ^a
Ni I	3515.049	0.109	−0.211	Blended ^a
Ni I	3524.535	0.025	0.008	Blended ^a
Ni I	3597.700	0.212	−1.100	Blended ^a
Ni I	3775.565	0.423	−1.393	Affected by Balmer line
Ni I	4231.027	3.542	−1.415	Blended with a CH line

^aBased on visual inspection of the VLT/UVES spectrum

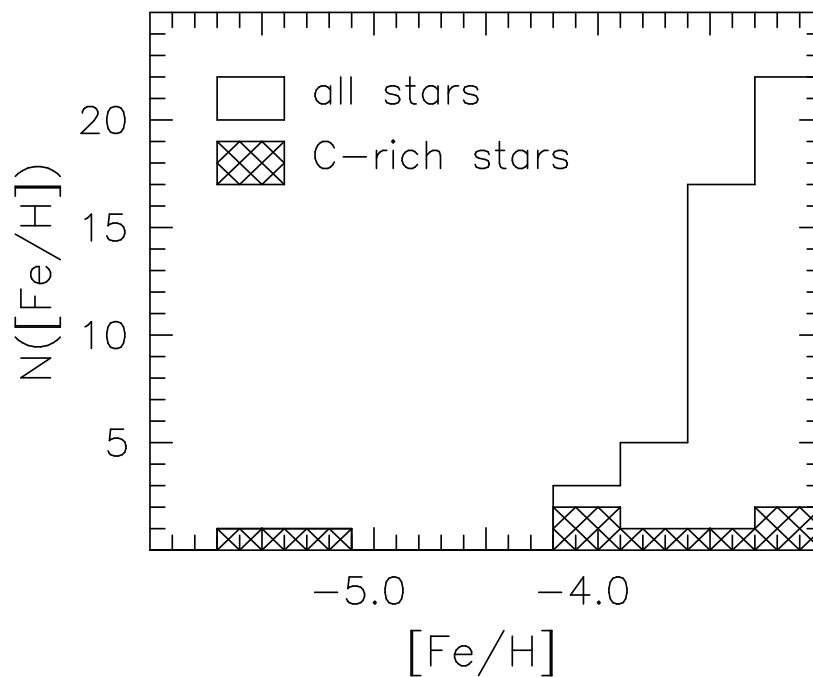


Fig. 1.— Histogram of $[\text{Fe}/\text{H}]$ for stars having high-resolution, high S/N , abundance analyses and $[\text{Fe}/\text{H}] < -3.0$, from the work of Aoki et al. (2002, 2004, 2006), Carretta et al. (2002), Cayrel et al. (2004), Cohen et al. (2004), Christlieb et al. (2002, 2004), Frebel et al. (2005, 2007b), McWilliam et al. (1995), Norris et al. (1997, 2000, 2001), Plez & Cohen (2005), and Ryan et al. (1991, 1996). Note that the proportion of carbon-rich objects increases dramatically as one moves to lower abundances.

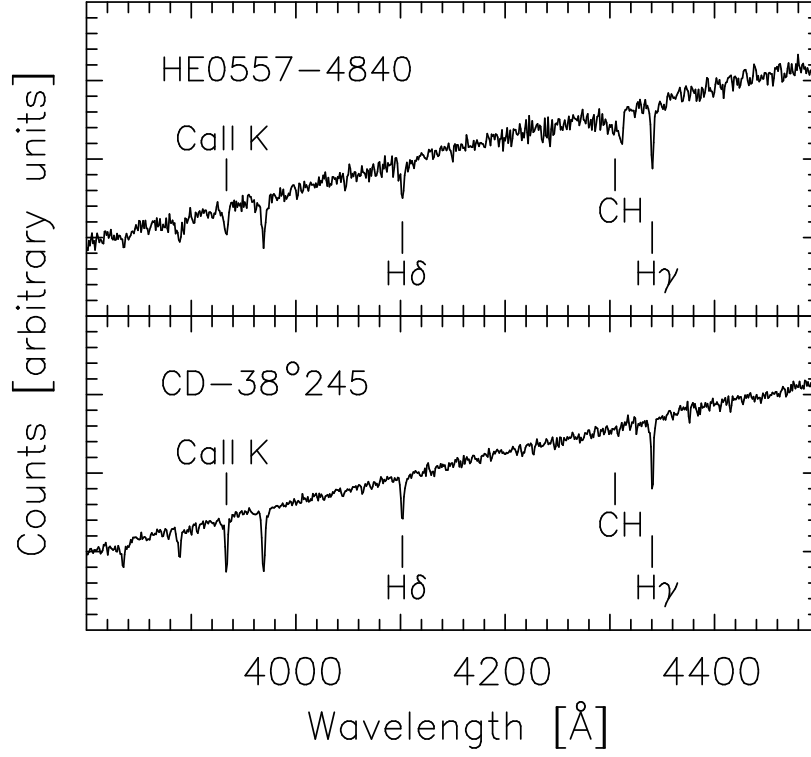


Fig. 2.— Medium resolution spectra of HE 0557-4840 and CD-38°245 ($[\text{Fe}/\text{H}] = -4.0$). Note that while the hydrogen lines have similar strengths in the two objects, the Ca II K line is weaker in HE 0557-4840, suggestive of a lower Ca abundance. Note also, however, that the G-band of CH is considerably stronger in HE 0557-4840.

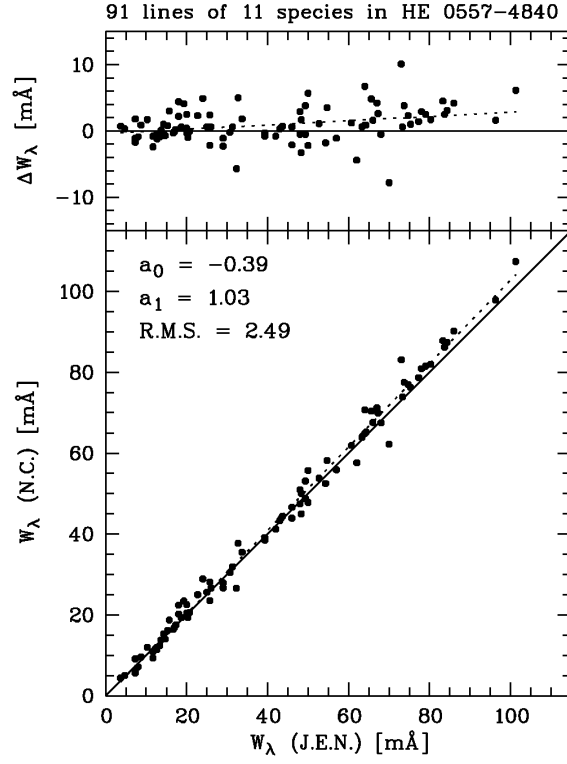


Fig. 3.— Comparison of equivalent width measured by N.C. and J.E.N. in the VLT/UVES spectrum of HE 0557–4840.

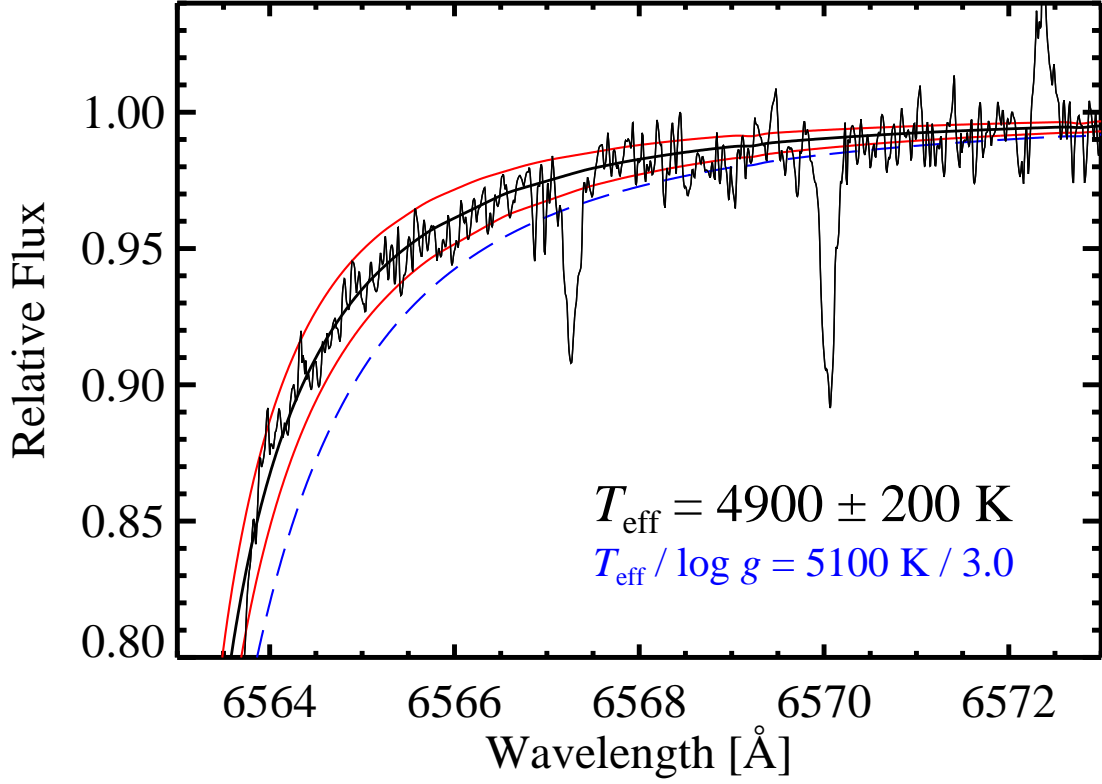


Fig. 4.— Comparison between the observed red wing of H α of HE 0557–4840 and synthetic spectra for $T_{\text{eff}} = 4700 \text{ K}$ (upper continuous line, in red), 4900 K (middle line, in black) and 5100 K (lower line, in red), top to bottom (all with $\log g = 2.2$). A synthetic profile for $T_{\text{eff}} = 5100 \text{ K}$ and $\log g = 3.0$ is also shown (dashed line, in blue, see §3.3). At the given signal-to-noise ratio, an effective temperature of $4900 \pm 100 \text{ K}$ (1σ) is indicated.

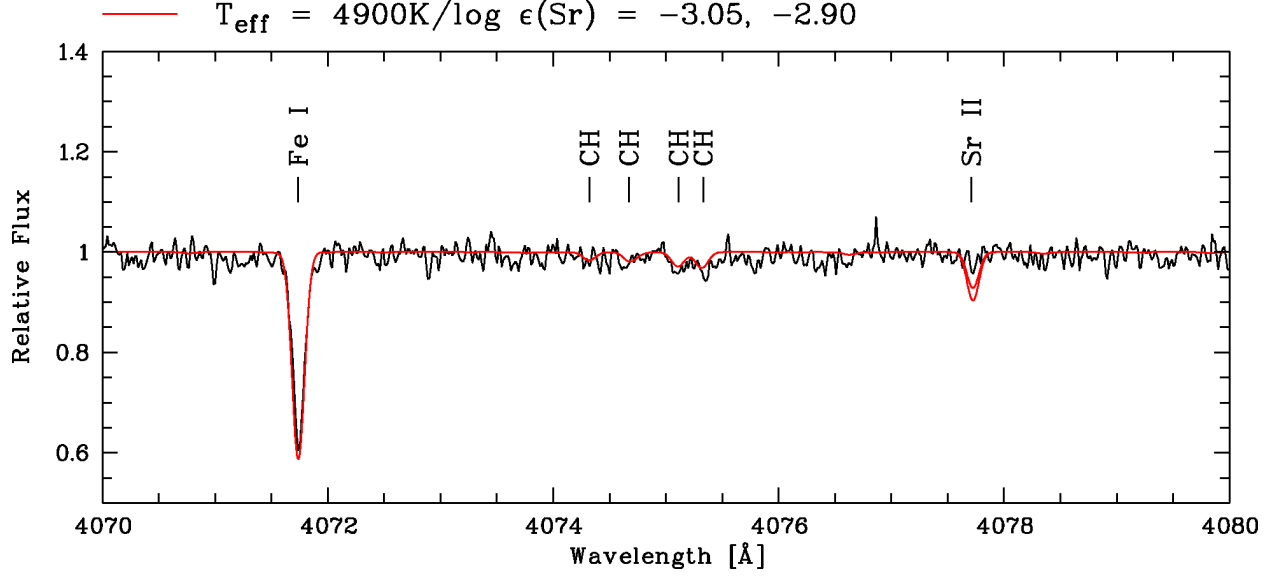


Fig. 5.— Spectrum synthesis of the Sr II 4077.71 line used to confirm the upper limit for the abundance of strontium. (The synthetic spectra (smooth red lines) have been broadened with a gaussian profile having $\text{FWHM} = 8.5 \text{ km s}^{-1}$, corresponding to $R = 35,000$.)

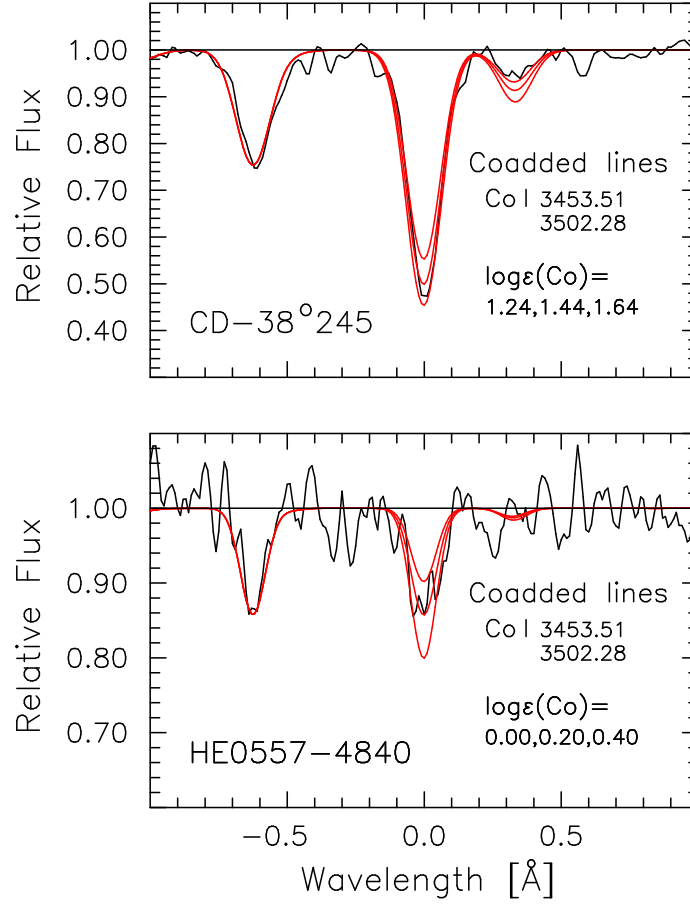


Fig. 6.— Comparison of observed and synthetic co-added spectra for the strongest two lines Co I lines in the interval 3400–3600 Å in CD-38° 245 and HE 0557–4840 (for $T_{\text{eff}} = 4900$ K). The lines co-added are identified, and the Co abundances given, in the figure. (The synthetic spectra (smooth red lines) for CD-38° 245 and HE 0557–4840 have been convolved with gaussian profiles having FWHM = 11.0 and 8.5 km s⁻¹, respectively, appropriate to the instrumental setups.) See text for details.

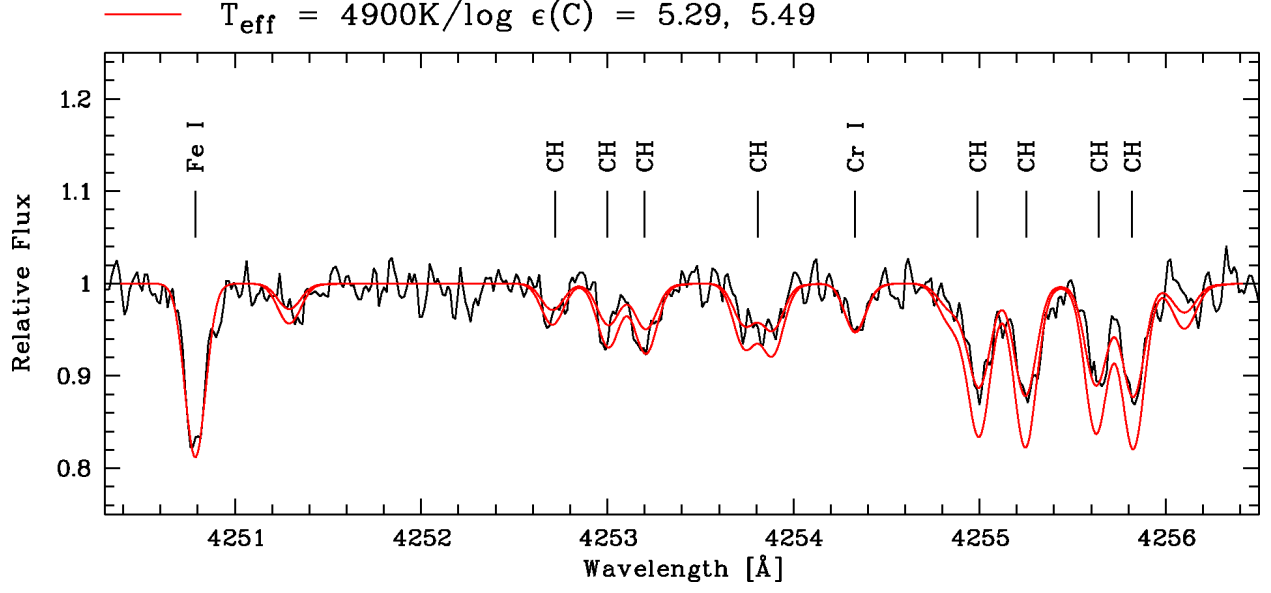


Fig. 7.— Spectrum synthesis (smooth red lines) of CH A-X lines in HE 0557–4840 for $T_{\text{eff}} = 4900$ K and carbon abundances of $\log \epsilon(\text{C}) = 5.29$ dex (best fit) and 5.49 dex.

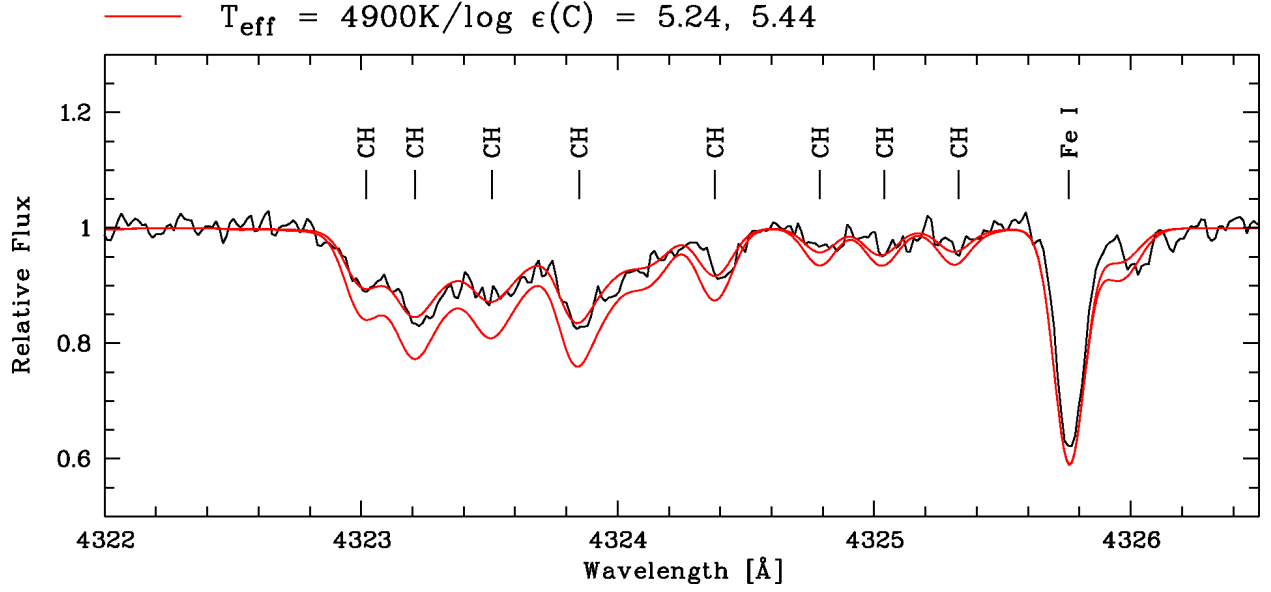


Fig. 8.— Spectrum synthesis (smooth red lines) of CH A-X lines in HE 0557–4840 for $T_{\text{eff}} = 4900\text{ K}$ and carbon abundances of $\log \epsilon(\text{C}) = 5.24\text{ dex}$ (best fit) and 5.44 dex .

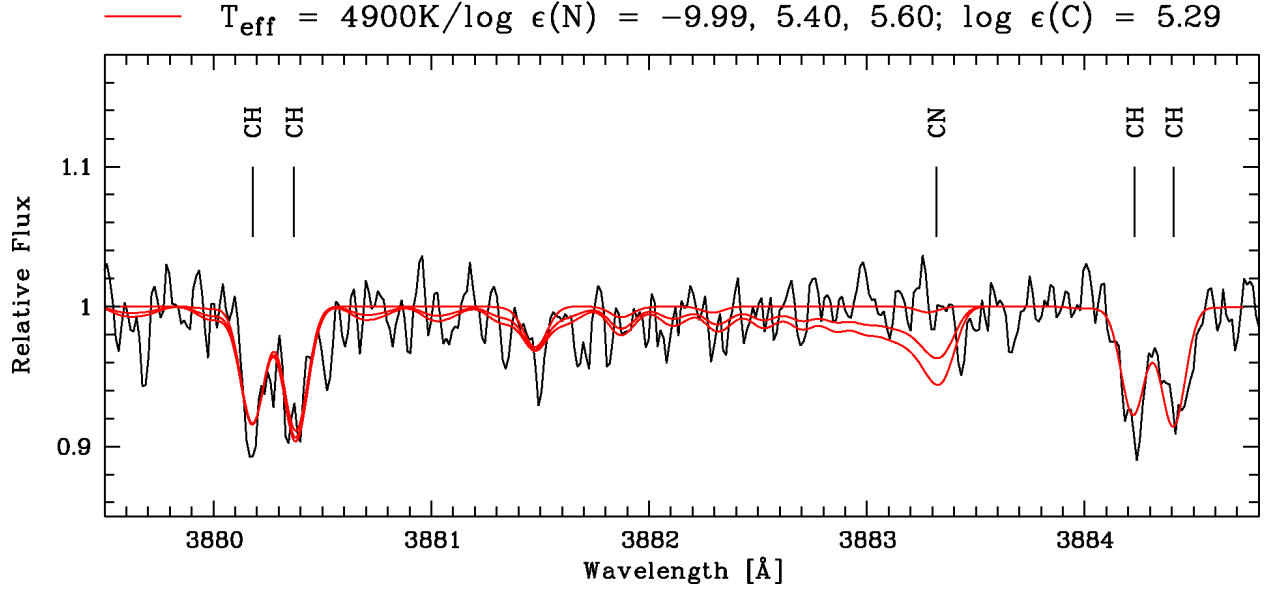


Fig. 9.— Spectrum synthesis (smooth red lines) of the (0,0) band head of the violet CN system in HE 0557–4840 for $T_{\text{eff}} = 4900\text{ K}$, $\log \epsilon(\text{C}) = 5.29$ and nitrogen abundances of $\log \epsilon(\text{N}) = -9.99$ (i.e., no nitrogen), 5.40 (adopted upper limit) and 5.60.

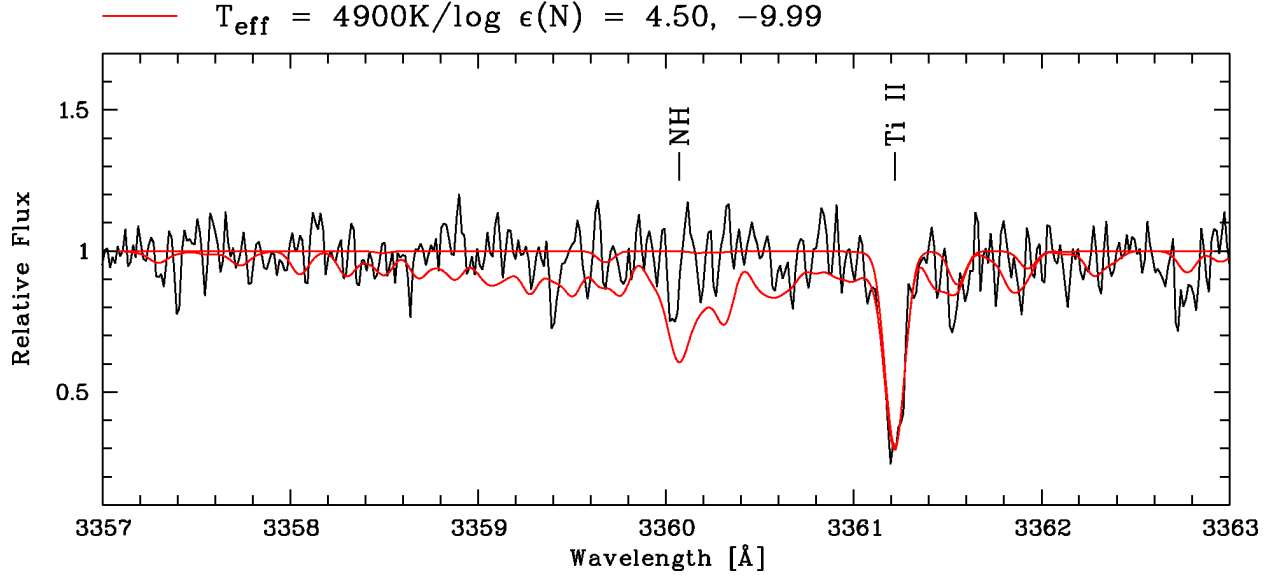


Fig. 10.— Spectrum synthesis (smooth red lines) of the NH band head for $T_{\text{eff}} = 4900\text{ K}$ and nitrogen abundances of $\log \epsilon(\text{N}) = -9.99$ (i.e., no nitrogen) and 4.50 (adopted upper limit).

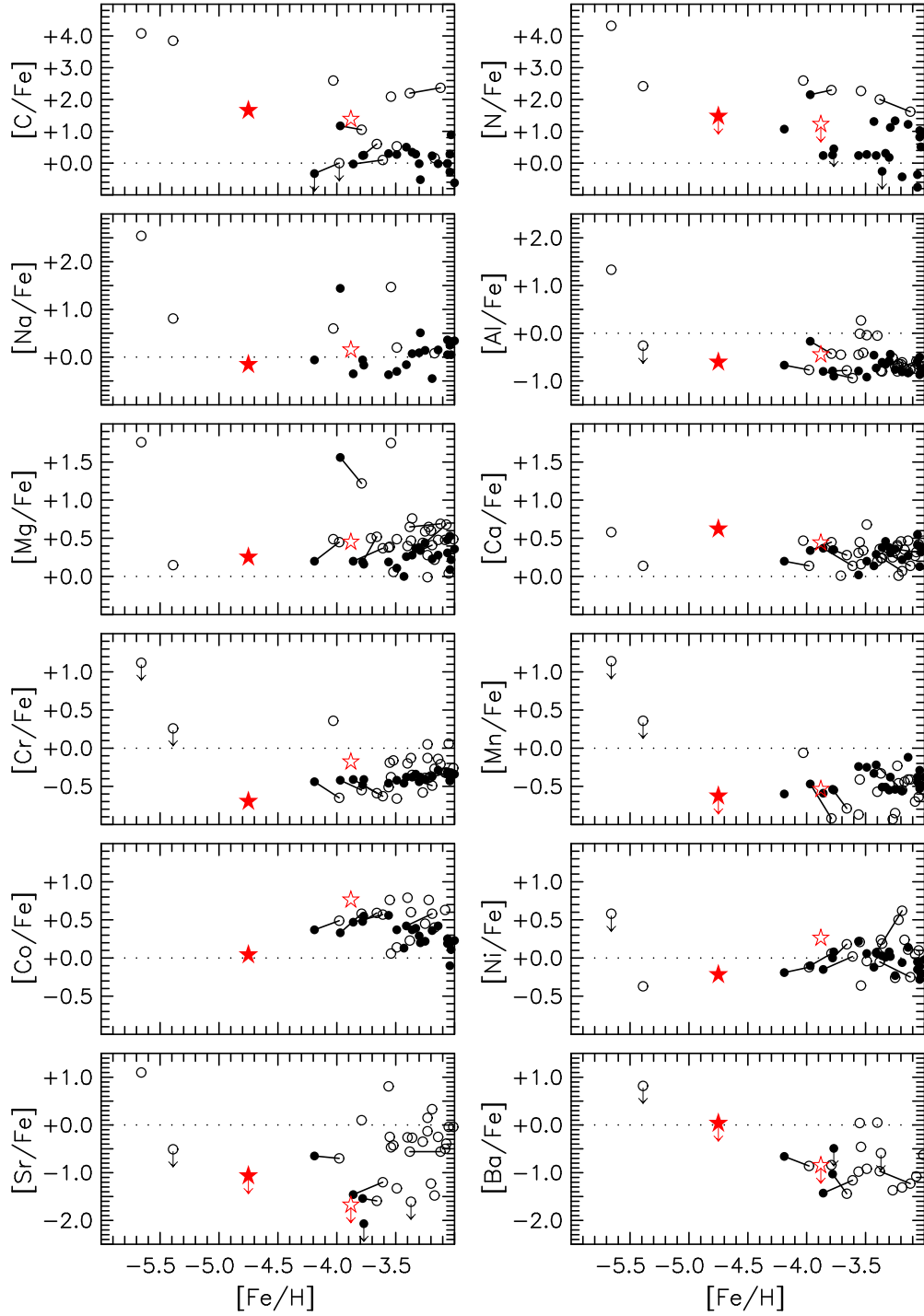


Fig. 11.— $[X/Fe]$ as a function of $[Fe/H]$. HE 0557-4840 is represented by a filled star while HE 1300+0157 (Frebel et al. 2007b) is shown by an open one. Filled circles represent results of Cayrel et al. (2004) and François et al. (2003), open ones those of Aoki et al. (2002, 2004, 2006), Carretta et al. (2002), Cohen et al. (2004), McWilliam et al. (1995), Norris et al. (1997, 2000, 2001, 2002), Plez & Cohen (2005), and Ryan et al. (1991, 1996).